**Geomorphology**
July 2023, Volume 433, Pages 108709 (20p.)
https://doi.org/10.1016/j.geomorph.2023.108709
https://archimer.ifremer.fr/doc/00836/94745/



# Using 17-years of beach-dune profile monitoring to characterize morphological dynamics related to significant extreme water level events in North Brittany (France)

Suanez S. [1, *], Yates M.L. [2, 3], Floc'h F. [4], Accensi Mickael [5]

[1] Univ Brest, CNRS, LETG UMR 6554, Institut Universitaire Européen de la Mer, rue Dumont d'Urville, 29280 Plouzané, France
[2] Laboratoire d'Hydraulique Saint-Venant, University Paris-Est and Cerema, 78401 Chatou, France
[3] Laboratoire d'Hydraulique Saint-Venant, Ecole des Ponts, EDF R&D, 78401 Chatou, France
[4] Univ Brest, CNRS, Geo-Ocean UMR 6538, Institut Universitaire Européen de la Mer, rue Dumont d'Urville, 29280 Plouzané, France
[5] Laboratoire d'Océanographie Physique et Spatiale, LOPS UMR 6523, Ifremer/CNRS/UBO/IRD, Z.I. Pointe du Diable, CS 10070, 29280 Plouzané, France

* Corresponding author : S. Suanez, email address : serge.suanez@univ-brest.fr

marissa.yates@enpc.fr ; france.floch@univ-brest.fr ; mickael.accensi@ifremer.fr

**Abstract :**

Long-term in situ monitoring of beach morphology is crucial for understanding the physical processes of coastal changes and defining the strategies of sustainable coastal management. Monthly surveys based on the beach/dune profile measurements started in July 2004 along six transects distributed along the Vougot beach (North Brittany). The analysis of these data from 2004 to 2021 shows that the eastern part of the beach has experienced chronic erosion during the 17-year period. This erosion has led to a lowering of the beach profile by about −1 to −1.5 m, and has resulted in the removal of beach sand such that waves now impact the underlying Holocene peat and Pleistocene silts or pebbles during most of the year. Conversely, the western part of the beach has accreted. Vougot beach is thus experiencing a rotation phenomenon characterized by a longshore sediment flux from the east to the west. The multidecadal evolution of the beach/dune system is punctuated by events causing significant retreat of the dune, especially when storm waves are combined with high spring tide levels. The event causing the most significant morphological changes was associated with extreme water levels (EWL) up to 9.6 m (i.e., Anne storm in February 2014), causing 14.5 m3 l.m−1 of dune sediment loss. The analysis of 17 years of hydrodynamic conditions (waves and water levels) indicates an increase in the wave runup height (+65 %) and EWL (+17 %). Calculation of the water level that exceeds the dune toe position (Δzexceedance) helps to further quantify the impacts of storm events on dune volume changes. The Anne storm had an EWL with a return period of approximately 9 years, but when combined with the dune toe position, showed the largest dune toe exceedance value (3.0 m), corresponding to a return period of approximately 20 years. Lastly, the events causing the most significant dune erosion during this 17-year study period have also caused shoreline erosion and/or landward barrier migration at many other sites in North Brittany, showing the broader scale impacts of observations at individual study sites.

**Highlights**

► Longshore sediment transport induces beach rotation. ► Long-term dune recovery trends are interspersed by significant erosion events. ► Sediment supply depletion in Brittany leads to long-term beach/dune erosion. ► Extreme Water Levels inducing significant erosion have return periods of 9 years. ► North Brittany coast behaves similarly to erosional extreme events.

**Keywords** : Surveys, Extreme water level, Beach/dune erosion, Sediment budget

## 1. Introduction

In recent decades, long-term surveying of beach morphological change and hydrodynamic conditions has contributed significantly to the study of beach and dune morphodynamics. Beach surveys were first undertaken to advance fundamental research to improve understanding of the governing physical processes of coastal erosion caused by storms, and finally of how to model beach evolution at a range of spatial and temporal scales (Davidson et al., 2013; Kroon et al., 2008; Yates et al., 2009; Masselink et al., 2016; Ostrowski et al., 2016; Mahabot et al., 2017; Dodet et al., 2019; Nicolae Lerma et al., 2022; Banno, 2023). At international scales, remarkable beach survey programs include the long-term (more than 30 years) monitoring of Narrabeen-Collaroy (Harley et al., 2011a; Turner et al., 2016) and Moruya (Thom and Hall, 1991; McLean and Shen, 2006) beaches in Australia, Duck beach (USACE) in North Carolina, USA (Mason, 1985; Howd and Birkemeier, 1987; Lee and Birkemeier, 1993), the Ogata (Tsuchiya et al., 1982; Karunarathna et al., 2015) and Hasaki (Banno et al., 2020) coasts of Japan, and the Dutch coastline (Louisse and van der Meulen, 1991; Wijnberg and Terwindt, 1995).

Surveys at Narrabeen-Collaroy and Moruya beaches in eastern Australia, started in 1976 and 1972 respectively (still on-going). These datasets were used to develop the international standard classification scheme used to describe the morphodynamic beach state as a function of the local wave climate, tide, and sediment characteristics (Wright and Short, 1984; Wright et al., 1987). They also significantly increased knowledge on surfzone rip current processes (Huntley and Short, 1992; Short and Hogan, 1994), the historical recurrence of extreme coastal erosion (Tamura et al., 2019), the beach/dune recovery processes after major storm events (McLean and Shen, 2006). By the beginning of the 2000's, these datasets were sufficiently long to study longer-term morphological changes caused by regional-scale meteo-oceanic forcing (Short and Trembanis, 2004; Ranasinghe et al., 2004; Harley et al., 2011b, Short et al., 2014), and they provide excellent, openly accessible databases to calibrate and test models of present and future sandy beach changes (Callaghan et al., 2008, 2009).

The DUCK beach monitoring program (*Displaying Underwater Conditions Kinematically*) has also contributed significantly to understanding coastal morphodynamics and beach modeling. It consisted of bi-weekly cross-shore beach and bathymetry measurements since 1981 (Mason, 1985; Howd and Birkemeier, 1987; Lee and Birkemeier, 1993), supplemented by a video monitoring system added in 1986 (Pianca et al., 2015). These data have allowed the advancement of theoretical knowledge in fields as varied as, (i) long-term evolution of beach profile and sediment budget related to the variation of meteo-oceanic conditions (Larson and Kraus, 1994; Reeve et al., 2007; Southgate, 2008; Zhang and Larson, 2021), (ii) nearshore sandbar behavior (Sallenger et al., 1985; Lippmann and Holman, 1990; Ruessink et al., 2003), (iii) estimation of the closure depth (Birkemeier, 1985; Nicholls et al., 1998), (iv) parameterization of wave setup and runup (Holman, 1986; Holland and Holman, 1993; Stockdon et al., 2006), and (v) validation of numerical models for simulating shoreline changes (e.g., Hanson, 1989).

In Japan, several study sites have benefited from long-term beach monitoring using piers, including the Ogata (1973-2008) (Tsuchiya et al., 1982; Karunarathna et al., 2015) and Ajigaura (1976-1998) (Hashimoto and Uda, 1982) coasts, based on monthly and weekly beach profile measurements, and the Hasaki coast since 1986 (Banno et al., 2020), based on beach profile measurements along a pier every weekday from 1986 to 2010 and weekly since 2010. The high frequency data set from Hasaki has been used to understand better (i) cyclic beach processes (Banno and Kuriyama, 2020), (ii) modeling longshore bar behavior (Ruessink et al., 2007; Pape et al., 2010), and (iii) the beach response to the El Niño–Southern Oscillation (ENSO) (Barnard et al., 2015).

Beach surveys may also be developed for coastal management programs (Ruggiero et al., 2000), such as coastal defense and shoreline adaptation in response to storm events and/or long-term sea-level rise impacts on the South Shore of Rhode Island since 1963 (Lacey and Peck, 1998), or along the Dutch coastline since 1990 (Hillen and Roelse, 1995; Koster and Hillen, 1995). The JARKUS database contains more than 30 years of beach profile measurements that has led to better understanding of the spatial and temporal evolution of the Dutch coastline (Louisse and van der Meulen, 1991; Wijnberg and Terwindt, 1995; Quartel et al., 2008), and to the development of a national shoreline preservation policy (Koster and Hillen, 1995).

In France, coastal monitoring is organized by a national program called SNO-DYNALIT (https://www.dynalit.fr/) that manages the long-term acquisition, archiving and distribution of topo-morphological data from about thirty selected study sites throughout France and the French overseas territories. Surveys of Truc Vert started in 1999 (Castelle et al., 2020) and have led to significant improvements in knowledge of (i) nearshore bar dynamics (Castelle et al., 2007, 2008; Almar et al., 2010), (ii) rip-current observations and modeling (Castelle and Ruessing, 2011), and (ii) shoreline changes including beach/dune system dynamics (Castelle et al., 2015, 2017). In Brittany, beach monitoring began at four study sites in the early 2000's, including the gravel spit barrier of Sillon de Talbert (Stéphan et al., 2018c; Suanez et al., 2018b), and the sandy beaches of Vougot (Suanez et al., 2016a, 2016b), Porsmilin (Jaud et al., 2019; Bertin et al., 2022) and Scucinio. These long-term observations were used to analyze beach and barrier processes including the impacts of storms on dunes and understanding and modeling macrotidal beach dynamics, including shoreline changes (Dehouck et al., 2009, Blaise et al., 2015; Stéphan et al., 2018b, 2019a; Suanez et al., 2012, 2015, 2018a; Floc'h et al., 2016; Lemos et al., 2018; Montaño et al., 2021).

In this paper, 17 years (2004-2021) of beach/dune profile surveys along 6 cross-shore transects located at Vougot beach (North Brittany) are analyzed (Fig. 1c). The goal is to study pluri-decadal beach/dune erosion and recovery phases in relation to the hydrodynamic conditions (storm waves combined with high spring tide water levels). First, morphological and sediment budget changes of the beach/dune system is analyzed. Secondly, an analysis of hydrodynamic conditions is completed to characterize the extreme events. The impact of these events (including extreme water levels) on the dune erosion is explored. Finally, the coastal processes at Vougot beach in terms of shoreline erosion are compared with other nearby beach surveys to characterize coastal morphodynamic changes along the North Brittany coast over the last two decades.

## 2. Study site and background studies

### *2.1. Morphological and hydrodynamical setting*

Vougot beach is located on the northern coast of Brittany, in the community of Guissény (Fig. 1a). It belongs to a large morphostructural unit covering the transition between

the plateau of Léon and the shelf-platform of the English Channel, consisting of a partly tectonic subaerial scarp 40 to 50 m high, which corresponds in some areas to an abandoned cliff (Battistini, 1955). Vougot beach is impacted by this morphostructural context since it is located in a collapsed tectonic compartment along two bounding faults oriented NW-SE (Fig. 1b). It is a large beach/dune system anchored on the abandoned cliff of Zorn that extends over about 2 km, oriented SW-NE (Fig. 1c). The Holocene dune complex accumulated since 3,250 cal BP and is 250 m to 400 m wide, culminating at 13 m a.s.l. (above sea level) (Guilcher and Hallégouët, 1991; Gorczyńska et al., 2023). The beach/dune system faces a 3 to 6 km wide platform scattered with reefs and islets (Fig. 1b,c), which constitute the resistant spots of the submerged granitic plateau of Léon subjected to intense weathering during the Tertiary (Battistini and Martin, 1956). These reefs and islets create a complex nearshore bathymetry and thus hydrodynamics (i.e., wave and currents) in the study area (Suanez et al., 2012; Dissanayake et al., 2021).

Vougot beach is a macrotidal beach (8.4 m spring tide range), with a 400 m wide intertidal beach. It consists of medium to fine sand, with $D_{50}$ ranging from 0.25-0.32 mm on the intertidal beach and 0.2 mm on the dune. However, on the eastern part of the beach, Pleistocene/Holocene pebbles and peat, or periglacial silt, may be seasonally uncovered when the overlying beach sand is removed (Battistini, 1954; Suanez et al., 2012; Chataigner, 2021). Offshore waves (see wave rose in figure 1a) show that energetic waves impact the coast from the W-N-W direction. The significant wave height ($H_{m0}$) is typically between 1 m and 1.5 m, and the peak period ($T_{pic}$) ranges between 9 and 10 s. The largest wave heights ≥ 10 m, and longest wave periods 18 s, occur in the winter (December-February) during energetic storms. The spring is characterized by less energetic wave conditions, with 36% of wave heights between 2 m to 4 m, and 34% of the wave periods between 8 to 12 s. The calmest wave conditions occur in the summer, before more energetic waves return in autumn with wave heights ~10 m approximately 20% of the time. The study area is protected from W to NW waves by the platform scattered with islets and reefs emerging at low tide (Fig. 1b,c). They cause significant wave refraction, shadowing, and diffraction as indicated by many "comet tails" formed in the lee of these obstacles (Fig. 1d).

*2.2. Previous studies*

A long-term study of shoreline changes using aerial photography demonstrated that the beach/dune system of Vougot beach experienced chronic shoreline retreat reaching about 0.7 m.y$^{-1}$ between 1978 and 2009 (Suanez et al., 2010a). This long-term erosion of the eastern part of the beach (e.g., profiles 1, 2, and 3, see figure 1c) is due to the construction of the Curnic jetty in 1974 that interrupted the westward sediment transport from Curnic to Vougot beach (Fig. 1c). This has caused a sediment deficit directly down drift of the jetty, along the eastern part of the beach. Significant storm events combined with spring high tide levels caused shoreline retreat of –6 m during the March 10, 2008 Johanna storm (Suanez and Cariolet, 2010b; Suanez et al., 2012), and –16 m during 2013-2014 stormy winter (Blaise et al., 2015; Masselink et al., 2016). Dune recovery phases that vary in time length are also observed, such as between 2008 and 2013 (Suanez et al., 2012; Suanez et al., 2015). During these periods, the dune/upper beach recovery is mainly due to cross-shore sediment transport from the lower to upper beach, which causes a significant reduction of sand along the lower-beach profile. Between 2008 and 2013, the shoreline prograded between 10 to 12 m (Stéphan et al., 2019a).

Using the beach classification of Masselink and Short (1993), Vougot beach is a non-barred dissipative beach. The surveyed cross-shore profiles typically show a steeper slope along the upper beach (~0.1) and a flatter slope along the lower-beach (~0.02), with a

transition occurring between the *Mean High Water Neap* and *Mean High Water Spring* tide levels (Suanez et al., 2015; Chataigner, 2021). The application of a simple, cross-shore empirical equilibrium-based shoreline change model (Lemos et al., 2018) at elevations ranging from –1 m to +6 m NGF (Chataigner, 2021) was able to reproduce well the observed erosion and accretion patterns in the upper intertidal ($R^2 > 0.6$) and the lower intertidal ($R^2 > 0.5$) zones. The cross-shore-only model represented a maximum of 50-60% of the shoreline position variance, emphasizing the importance of longshore processes at this site.

More recently, a study conducted by Montaño et al. (2021), analyzed the beach/dune profile changes along the eastern part of the beach (profiles 1, 2, and 3) through a centroid analysis. The authors showed that the erosion and recovery phases resulted from complex long-term and short-term interactions between the dune and the beach. The long-term trend was characterized by profile steepening (due to the lower beach retreating and the upper beach advancing), which was interrupted by episodic storm events causing profile flattening (lower beach advancing and upper beach retreating).

## 3. Data and methods

### *3.1. DGPS topo-morphologic measurements*

The topo-morphological surveys consist of monthly beach/dune profile measurements along 6 transects distributed from east to west along the beach (Fig. 1c,d). However, the approximately monthly survey frequency was adapted to the hydrodynamic conditions, with post-storm surveys completed just after major storm events inducing significant dune erosion. Measurements at the eastern (profiles 1, 2, and 3) and western (profiles 4, 5, and 6) ends of the beach began in July 2004, and June 2011, respectively (Suanez et al., 2016a). The origin of each profile measurement (i.e., "head of profile"), is indicated by a 2 m long galvanized tube driven into the dune.

In addition to the beach/dune profile measurements, the shoreline position along the entire beach is also measured annually (Suanez and Blaise, 2016). The shoreline proxy used here is defined by the bio-morphological criterion associating the morphology and the vegetation (*Elymus farctus*) limit of the dune (Boak and Turner, 2005), which generally agrees with the shoreline dynamics. When the dune is accreting, the vegetation colonizes the seaward slope, prograding toward the sea. Conversely, when the dune is eroding, wave attack often forms erosion scarps causing the retreat of the vegetation limit. Topographic surveys were completed with a DGPS (Suanez et al., 2010a), which was calibrated using a geodesic marker from the French datum and the geodesic network provided by the IGN (*Institut Géographique National*). Five ground control points (GCP), in addition to the heads of the six profiles, were installed in the field to evaluate the survey accuracy (Fig. 1c). The errors for each GCP are calculated with the standard deviation, showing a horizontal and vertical accuracy of ±2-3 cm and ±1 cm, respectively.

### *3.2. Beach/dune profile analysis*

In addition to analyzing the topo-morphological changes for all profiles, the sediment budget was analyzed by dividing the beach/dune system of each profile in two sections. First, the entire beach/dune volume evolution was calculated using the most seaward measurement in all profiles as the lower beach boundary (Table 1). Second, the sediment budget evolution was calculated only for the dune section. For each profile, the lower boundary of the dune was determined from the first survey showing a distinct slope break between the dune and the

upper beach. For both analyses, these limits were kept fixed to calculate sediment budgets within a virtual box of constant area (Fig. 2a).

The calculation of the sediment volume (in volume per linear meter) is based on the topographic vertical change between each profile measured at time $t_i$ and $t_{0.}$(original profile). The profiles were gridded at a horizontal resolution of 0.25 m. Using Eq. (1), the area ($S_{Nj},t_i$ for $j$=1,$m$) between the profile at date $t_i$ ($i$=0,$n$) and an arbitrary reference "sand" level (e.g., –10 m) was calculated, taking into account each intersection node $N_j$ ($x_j$), by defining the zones of erosion and accretion between two subsequent surveys (Fig. 2b):

$$S_{N_j,t_i} = \int_{-10}^{h(t_i)} dz \int_{x_{j-1}}^{x_j} dx \qquad \text{Eq. 1}$$

where $j$=0,$m$, $x_j$ is the cross-shore position of node $N_j$ ($x_0$ is distance 0, and $x_m$ is the position of closure of each section, as defined by the intersection node $N_m$), and $h(t_i)$ is the sand level measured at $x(t_i)$.

The total change between subsequent survey dates is calculated as:

$$\Delta S_{N_j,t_{i+1}} = \int_{-10}^{h(t_i+1)} dz \int_{x_{j-1}}^{x_j} dx - \int_{-10}^{h(t_i)} dz \int_{x_{j-1}}^{x_j} dx \qquad \text{Eq. 2}$$

The node-to-node area budgets representing the sediment eroded or accumulated (negative or positive) are then summed over the entire profile to obtain the total volume budget $\Delta V_{t_i+1}$ per linear meter alongshore.

$$\Delta V_{t_i+1} = \Delta S_{t_i+1} = \sum_{j=1}^{m} \Delta S_{N_j,t_i} \qquad \text{Eq. 3}$$

where the cumulative volume budget $\sum_1^n \Delta V_{t_i+1}$ is the sum of the sediment budget over the entire survey period.

*3.3. Offshore wave modeling*

Offshore wave data from July 1, 2004 to December 31, 2021 were obtained from the ResourceCode hindcast data set (Accensi et al., 2021; Accensi, 2022), developed by the Ifremer. The hindcast is generated with the WAVEWATCH III (WW3) version 7.08 (WW3DG, 2019) spectral model, which uses higher resolution grids in the coastal zone, but is still unable to capture fully wave transformation over the complex nearshore bathymetry. Hourly wave time series of the significant wave height ($H_{m0}$), mean period ($T_{m-1,0}$), and mean direction ($\theta$) were compared at two model nodes located at the western (node 138170 at 48.655319°N; –4.510499°W, in 21 m depth), and eastern (node 138362 at 48.668049°N; –4.481347°W, in 22.1 m depth) ends of Vougot beach (Fig. 1b). The mean and standard deviation of the differences in wave height $H_{m0}$ (–0.003±0.17 m), period $T_{m-1,0}$ (–0.1±0.26 s), and direction (9.5°±6.9°) are small (Fig. 3), indicating that the offshore wave conditions (~20 m depth) are similar at the eastern and western ends of the nearshore zone.

The wave energy flux $F$ was calculated as (see Tucker and Pitt, 2001):

$$F = \frac{\rho g^2 H_{m0}^2 T_{m-1,0}}{64\pi} \qquad \text{Eq. 4}$$

where $F$ is expressed per unit crest length of the wave (in $J.m^{-1}s^{-1}$), $\rho$ = 1,025 $kg.m^{-3}$ is the density of seawater, and $g$ = 9.81 $m.s^{-2}$ is the gravitational acceleration. The wave energy flux takes into account both the wave height ($H_{m0}$) and period ($T_{m-1,0}$) and is used as an additional criteria to evaluate significant coastal storm impacts.

*3.4. Water level measurements*

High frequency in-situ water levels were measured using an OSSI-010-003C, (Ocean Sensor Systems Inc.®) pressure sensor recording at 5Hz, deployed at –2.48 m depth (i.e., lower intertidal beach), along profile 1 (Fig. 1c) from June 5, 2012 to April 6, 2018 (Suanez and Floc'h, 2018). The data were corrected with the atmospheric pressure recorded at the Brignogan Météo France station (Fig. 1a) and for the non-hydrostatic pressure using linear wave theory (e.g., Hom-ma et al., 1966; Bishop and Donelan, 1987). The mean surface elevation was extracted using a 10-minute moving average.

The tide dataset was provided by the SHOM (*Service Hydrographique et Océanographique de la Marine*) through the open access database REFMAR-data-SHOM. The dataset corresponds to the hourly observed tide recorded at the Roscoff station located approximately 36 km east of Vougot beach (Fig. 1a).

The tide level at Vougot beach was estimated using the method of tidal concordance (George and Simon, 1984) between the Roscoff tide gauge (i.e., reference site) and the pressure sensor measurements at Vougot beach (i.e., secondary site). For a given amplitude of the tide at the reference site, the corresponding amplitude and phase shift was estimated at the secondary site (Simon et al., 2013). The high tide (HT) and low tide (LT) water levels observed during each tidal cycle were compared between the two sites for the 6-year measurement period. Using low tides only or both high and low tides to calculate the linear regression between the two sites produced similar results, with RMSE of 0.14 m and 0.07 m, respectively. The most reliable estimate is typically the regression using only LT levels (to avoid including nonlinear effects at HT at the secondary site). However, since nonlinear effects were not observed at Vougot beach, the HT+LT linear regression :

$$WL_{Vougot} = 0.92\, WL_{Roscoff} + 0.09 \qquad \text{Eq. 5}$$

was used since the HT water levels are the focus of this work.

*3.5. Extreme water levels and dune erosion assessment*

As shown by Ruggiero et al. (2001), the likelihood of dune/shoreline erosion is based on comparing the extreme water level (*EWL*) with the measured elevation of the junction between the upper beach face and the dune, called the dune toe elevation here. The total *EWL* elevation is due to a combination of different physical processes:

$$EWL = predicted\ tide + surge + wave\ runup\ (\eta + R) \qquad \text{Eq. 6}$$

where *surge* is the result of the atmospheric forcing (pressure and wind), and *wave runup* is the sum of the wave setup ($\eta$) and the swash elevation ($R$).

In previous work, Cariolet and Suanez (2013), and Suanez et al. (2015) calibrated a *wave runup* equation for Vougot beach based on the Hunt (1959) and Battjes (1974) formula:

$$\frac{R}{H_{m0}} = C\xi \quad \text{Eq. 7}$$

where $C$ is a nondimensional constant, and $\xi$ is the *Iribarren number* given by:

$$\xi = \frac{tan\beta}{\sqrt{H_{m0}/L_0}} \quad \text{Eq. 8}$$

where the beach slope tan$\beta$ was computed on a time-varying section of the cross-shore profiles using the high tide water level (*HTWL*) and a fraction of the wave height ($H_{m0}$) to calculate the upper and lower bounds of the profile section:

$$Bound_{\text{up and low}} = HTWL \pm 1/4H_{m0} \quad \text{Eq. 9}$$

and $L_0$ is calculated using linear wave theory:

$$L_0 = \frac{gT_{m-1,0}^2}{2\pi} \quad \text{Eq. 10}$$

where $T_{m-1,0}$ is the energy mean wave period and $2\pi/T$ is the radian frequency.

The wave conditions used Eq. 7 and 10 were extracted from the hindcast simulations in approximately 20 m water depth, following the approach of Holman (1986) and Holman and Sallenger (1985). At this depth, the effects of the complex offshore bathymetry are taken into account, while remaining within the range of water depths recommended for spectral wave models. Note that some other authors deshoaled these wave conditions to use the deep water wave height $H_0$ in the calculation of wave runup (e.g., Stockdon et al., 2006; Didier et al., 2020).

Cariolet and Suanez (2013) and Suanez et al. (2015) proposed a nondimensional constant $C$ between 0.67 and 0.68 based on field swash runup measurements at profile 1 (see Fig. 1c,d), and WWW3 wave conditions extracted at –18.3 m depth. In this study, the value of $C$ was recalibrated since an updated wave hindcast data set was used, and wave conditions were extracted at a different location (in –22.1 m depth), resulting in the following estimate of wave runup:

$$R_{max} = 1.0\, H_{m0}\xi \quad \text{Eq. 11}$$

with $R^2 = 0.77$ and RMSE = 0.37 m in comparison to the measurements, which is consistent with the results ($R^2 = 0.81$ and RMSE = 0.33 m) obtained by Suanez et al. (2015).

Finally, as proposed by Ruggiero et al. (2001) the evaluation of the impact of waves on dune erosion was based on the *EWL* "exceedance", i.e., when *EWL* exceeds the elevation of the dune toe $z_{dunetoe}$. As described in section 3.2, $z_{dunetoe}$ corresponds to the limit between the upper beach and dune. The dune toe exceedance $\Delta z_{exceedance}$, was thus calculated as:

$$\Delta z_{exceedance} = EWL - z_{dunetoe} \quad \text{Eq. 12}$$

Positive $\Delta z_{exceedance}$ values indicate that the *EWL* impacts the dune and can cause erosion.

## 4. Results

*4.1. Beach/dune profile changes*

Along the eastern side of the beach, the envelopes of profiles 1, 2 and 3, show similar evolution characterized by vertical erosion of –1 to –1.5 m along the lower beach, causing significant horizontal retreat of the dune front, ranging from –5 to –10 m (Fig. 4). As indicated by Montaño et al. (2021), this long-term trend of beach profile changes induced profile steepening and rotation at elevations between the mean high water spring (MHWS) and the highest astronomical tide (HAT) levels. The most significant morphological changes occurred mainly along the dune section, with the standard deviation σ of vertical changes reaching ±0.75, ±0.95, and ±1.3 m for profiles 1, 2, and 3, respectively (Fig. 4).

In contrast, along the western part of the beach, profiles 5 and 6 accumulated sediment along both the dune and the intertidal beach, reaching about +0.5 m of vertical change. This caused a horizontal advance of the dune for both profiles, reaching +3 to +4 m (Fig. 4), causing significant vertical changes with σ = ±0.5 and ±0.75 m for profiles 5 and 6, respectively. In both cases, the flattening of the beach profile due to accretion along the intertidal beach shows that the inflection point is situated around the mean high water neap (MHWN) level, i.e., at a lower level than for the three previous profiles 1, 2, and 3.

Profile 4, situated in the transition zone between the eastern (eroding) and western (accreting) zones, experienced –1.75 m of dune retreat, while the intertidal beach profile remained stable over the entire survey period (Fig. 4). The most significant morphological changes occurred on the dune with σ of about ±1.15 m (vertically).

Morphological changes occurred along all sections of the beach/dune for all 6 profiles, but with different magnitudes (Fig. 5). The vertical variations of the intertidal beach range between 1 and 1.4 m for profiles 1, 2, and 3 but only 0.5 and 0.6 m for profiles 4, 5, and 6. However, the largest changes occurred on the dune, reaching between 4.3 and 4.7 m for profiles 1, 2 and 3, illustrating the significant retreat of the dune on the eastern part of the beach. To the west, the largest morphological changes of the dune reached 3.6, 2.1, and 2.7 m for profiles 4, 5 and 6, respectively (Fig. 5). However, for profiles 5 and 6, these values illustrate the accretion/progradation on the dune.

*4.2. Sediment budget of the beach/dune system*

The sediment analysis of the beach/dune system shows that the eastern part of the beach lost between –100 and –120 $m^3$ $l.m^{-1}$ (cubic meters per linear meters) over the 17-year survey period (Fig. 6a). The cumulative curve suggests the sediment loss was nearly linear, with linear regressions showing –4.7 $m^3.yr^{-1}$ ($R^2$ = 0.88), –5.3 $m^3.yr^{-1}$ ($R^2$ = 0.95), and –7.2 $m^3.yr^{-1}$ ($R^2$ = 0.88) for profiles 1, 2 and 3, respectively. In the middle of Vougot beach (i.e., profile 4), the sediment budget between 2011 and 2021 lost –60 $m^3$ $l.m^{-1}$, and the trend in sediment loss varied more in time, with –5.3 $m^3.yr^{-1}$ ($R^2$ = 0.46) (Fig. 6a). On the western part of the beach (i.e., profiles 5 and 6), the sediment budget of the beach/dune system between 2011 and 2021 gained +29 and +85 $m^3$ $l.m^{-1}$, respectively (Fig. 6a). Although the strong variations in sediment budget evolution along profile 5 suggest that the trend is not significant, the annual sediment gain of +8 $m^3.yr^{-1}$ along profile 6 appears significant (linear trend, $R^2$ = 0.95).

These observations agree with the beach/dune profile changes, showing significant accretion/progradation and erosion/retreat of the beach/dune at the western and eastern ends of the beach, respectively (Fig. 4). The total sediment budget shows that the eastern zone (e.g., profiles 1, 2, 3) has eroded significantly. The erosion rate decreases moving toward the center of the beach (e.g., profile 4), before the sediment budget becomes positive in the

western zone (e.g., profiles 5 and 6), especially along profile 6, where it increased significantly over the survey period.

*4.3. Sediment budget of the dune section*

The dune sediment budget over the survey period (2004-2021) shows an increasing sediment deficit from profile 1 to 3 reaching –6.8, –9.8, and –32.7 $m^3$ $l.m^{-1}$, respectively (Fig. 6b). This is consistent with the dune retreat observed from changes in the beach/dune profiles (Fig. 4). However, these changes do not show a linear trend, but instead are characterized by significant, episodic erosion events, followed by longer, slower recovery phases (of variable time length) of dune sediment volume increasing. The dune sediment budget at the center of the beach (i.e., profile 4) decreased by –17.8 $m^3$ $l.m^{-1}$ between 2011 and 2021, while it increased to the west (i.e., profiles 5 and 6) by +9.2 and +16 $m^3$ $l.m^{-1}$, respectively (Fig. 6b).

Approximately ten significant erosion phases are identified (Fig. 6b), with varying magnitudes for each profile. The profiles located along the eastern end and center of the beach (e.g., profiles 1, 2, 3, and 4) experienced significant erosion. When moving to the west (profiles 5 and 6), these erosion phases were less frequent and showed smaller or no losses of sediment. The most erosive event clearly identifiable along all 6 profiles occurred on February 4, 2014 (Table 2). However, the significant erosion events are typically followed by a dune recovery phase lasting until the next erosion event (Fig. 6b), as was the case after the Johanna storm on March 10, 2008 (Suanez et al., 2012).

*4.4. Hydrodynamic conditions*

To identify events potentially causing significant morphological changes, the wave and water level time series were analyzed. The 99.9$^{th}$ quantile significant wave height (at node 138362, see section 3.3.), $H_{m0}$ = 6.7 m of the 17-year time series was used as a threshold to identify energetic wave events (Fig. 7a). Assuming that values exceeding this threshold within a 48-hour time period belong to the same storm event, 20 significant events were identified (Fig. 7a). The 99.9$^{th}$ quantile wave energy flux (Eq. 4), $F = 7.4x10^5$ $Jm^{-1}s^{-1}$, corresponding to the 99.9$^{th}$ quantile of $H_{m0}$ and $T_{m-1,0}$ of 15.5 s (i.e., mean ($\bar{x}$) plus one standard deviation ($\sigma$) $T_{m-1,0}$ associated with $H_{m0} \geqslant$ 99.9$^{th}$ quantile) was also used as a threshold to take into account the effects of the wave period. By considering the wave energy flux, the number of significant events was reduced from 20 to 13 (Fig. 7b).

Energetic wave events typically have the strongest morphological impacts on the dune when they occur during high spring tides (Carter et al., 1990; Ruggiero et al., 2001). The simultaneous occurrence of the wave height $H_{m0}$ and observed tide level exceeding the 97$^{th}$ quantiles (choice of threshold iteratively tested) enabled identifying 11 major events (see table 3 and vertical red lines in figure 7c) that generated significant dune erosion (as shown in table 2). Several of the large significant wave height or wave energy flux events shown in figure 7a,b are not identified in the joint analysis, whereas some less energetic storms are identified due to the joint occurrence of a high water level.

*4.5. Dune erosion assessment under extreme morphogenetic conditions*

The assessment of dune erosion was based on the simple model of Ruggiero et al. (2001), by comparing the extreme water level (*EWL*) to the dune toe elevation. This analysis was conducted along profile 1 since the estimation of wave runup (Eq. 11) was calibrated using observations from profile 1 (see section 3.5). The estimation of the *EWL* was calculated using Eq. 6 for both daily high tides (Fig. 8). The beach slope parameter $\tan\beta$ (Eq. 9) and the

dune toe elevation were calculated/extracted from the most recent beach profile measurement, remaining constant between survey dates.

Approximately 150 *EWL* events exceeded the dune toe position ($\Delta z_{exceedance} > 0$) over the 17-year time period (Fig. 8c). Comparisons of the dune toe exceedance $\Delta z_{exceedance}$ (mean, standard deviation, or integrated sum between survey periods) and dune sediment budget changes $\Delta V_{dune}$ showed no significant correlations. Additional parameters representing the integrated erosion-only $\Delta z_{exceedance}$, the duration of erosional $\Delta z_{exceedance}$, or the ratio of these quantities to those calculated for accretional $\Delta z_{exceedance}$ (i.e., $\Sigma\Delta z_{exceedance\_erosion}$ / $\Sigma\Delta z_{exceedance\_accretion}$) were also tested without demonstrating any significant correlations.

However, the hypothesized relationship is observed when comparing the time periods characterized by a negative dune sediment budget (erosional phases) and the occurrence of *EWL* events causing dune toe exceedance. Significant events were defined as erosion (accretion) values with a magnitude larger than the mean ($\bar{x}$) ± 0.5 times the standard deviation ($\sigma$), and are highlighted in gray in figure 8c,d, showing that $\Delta z_{exceedance}$ may be used as a proxy to estimate *EWL* events that will cause erosion, in particular in the case of large $\Delta z_{exceedance}$.

The probability and cumulative density distributions of the dune toe exceedance $\Delta z_{exceedance}$ show that the *EWL* remains far below the dune toe the majority of the time (e.g., $\Delta z_{exceedance} < -2$ m more than 80% of the time) and surpasses the dune toe only on rare occasions (e.g., $\Delta z_{exceedance} > 0$ m less than 4% of the time) (Fig. 9). The full time series separated into positive (accretion, blue) and negative (erosion, red) dune sediment budget time periods, shows a qualitative relationship between $\Delta z_{exceedance}$ and $\Delta V_{dune}$. Therefore, one simple approach is to assume that the dune sediment volume changes are linearly proportional to the dune toe exceedance, with different erosion and accretion rates:

$$\Delta V_{dune\_est} = C^{+}\,\Delta z_{exceedance}\,(\Delta z_{exceedance} < 0) + C^{-}\,\Delta z_{exceedance}\,(\Delta z_{exceedance} > 0) \qquad \text{Eq. 13}$$

where $C^{+}$ and $C^{-}$ represent the dune accretion and erosion transport rates, respectively, as a function of the dune toe exceedance (i.e., $\Delta z_{exceedance} < 0$ for $C^{+}$, and $\Delta z_{exceedance} > 0$ for $C^{-}$). By minimizing the difference between the measured ($\Delta V_{dune}$) and estimated ($\Delta V_{dune\_est}$) dune volume changes, $C^{+}$ and $C^{-}$ were determined using a least squares linear regression for different thresholds of significant values of $\Delta z_{exceedance}$ (ranging from 0 to 2m).

The objective here is not to develop a model to accurately predict dune sediment volume changes, but to evaluate the impacts of *EWL* on dune evolution. The $R^2$ correlation coefficients between the measured and estimated dune sediment volume changes range from 0.37 to 0.55, with the maximum obtained for a $\Delta z_{exceedance}$ threshold of 1.1 m. The optimal $C^{+}$ and $C^{-}$ coefficients differ by approximately 3 orders of magnitude (i.e., for a threshold of 1.1 m, $C^{+} = -0.007$ $m^3$ $l.m^{-1}$ $m^{-1}$ and $C^{-} = -1.37$ $m^3$ $l.m^{-1}$ $m^{-1}$, indicating the amount of dune volume change per meter of dune toe exceedance), highlighting the significant differences in dune response to different physical forcing during erosion (hydrodynamic) and accretion (aeolian) phases.

## 5. Discussion

### *5.1. Beach « rotation » processes*

The difference in beach/dune profile changes along the eastern and the western ends of Vougot beach is also observed in the long-term shoreline changes. Between 2000 and 2021, the shoreline changes (Fig. 10a) showed a maximum retreat of –20 m (corresponding to –0.95 $m.yr^{-1}$) in the east, and progradation reaching +14 m in the west (Fig. 10b). This beach

rotation phenomenon induces a linearization of the coastline, causing the removal of the protuberance located between profiles 3 and 4. It corresponds to a "relic" tombolo-like form that developed in the sheltered zone of the islet of Enez Du, showing that Vougot beach originally formed (i.e., during the Holocene sea level rise) from both cross-shore and longshore sediment transport processes. It can be hypothesized that it was anchored to the islets located in front of the current coast during lower sea levels, then retreated to its present position with sea-level rise. The cross-shore dynamics are still clearly observed by the numerous comet tail accumulations behind islets and reefs. However, the construction of the Curnic jetty in 1974, which caused an interruption of the sediment transit between the beaches of Curnic and Vougot (see section 2.2.), exacerbated the erosion of the protuberance causing the shoreline to straighten (Suanez et al., 2010a) (Fig. 10b,c). The largest erosion rates are currently observed in the east, which no longer has a source of sediments, and longshore currents transport the eroded sediment to the west.

As noted by Banno (2023), short-term, high-frequency surveys may be sufficient to evaluate morphological changes caused by cross-shore sediment transport, but long-term monitoring is needed to analyze morphological changes caused by both cross-shore and longshore sediment transport. Short et al. (2014) indicated that six years of data was insufficient to detect long-term trends observed at Narrabeen beach since 1976, however, it helped to detect beach rotation in response to the local and regional hydrodynamic conditions. At Vougot beach, 17 years of high frequency surveys agree with the multi-decadal rotation of the beach, at least since the Curnic jetty was built in 1974 (Suanez et al. 2010a).

*5.2. Hypothesis of longshore current and sediment transport*

The meteorological and hydrodynamic conditions suggest favorable conditions for the generation of a coastal current flowing from east to west. Strong winds are observed from the E-N-E (60°) essentially in spring and to a lesser extent in autumn (see Suanez et al., 2012), with speeds > 8 $m.s^{-1}$ (Fig. 11a), generating waves propagating to the SW (Fig. 11b). This is consistent with the estimates of the wave propagation direction during significant events (Table 3).

The morphology of the offshore and nearshore zone in front of Vougot beach also induces significant changes in coastal wave propagation due to the presence of islands, islets and reefs (see figure 1 and section 2). Aerial photographs of the eastern part of the beach (Fig. 11c) show wave refraction and diffraction around islets, inducing a wave breaking angle α oriented to the west and thus longshore currents from the east to the west (Fig. 11c). Ebb tidal currents flowing from the NE to the SW may also play an important role (Fig. 11d) by interacting with wave-induced currents in the nearshore zone, potentially influencing the magnitude and even direction of the nearshore sediment transport. Measurements of intertidal/shoreface zone currents are necessary to confirm these hypotheses.

As indicated by Gallop et al. (2020), geologically controlled beaches are a distinct beach type, and have their own unique morphodynamic processes that make them behave differently to unconstrained beaches. Therefore, in contrast to surveys carried out on open coasts that are characterized by more uniform sandy offshore zones (i.e., the study sites of Moruya, Duck, Truc Vert, Hasaki, etc., indicated in the introduction), the offshore platform scattered with islets and reefs adjacent to Vougot beach creates more complicated morphodynamic processes. The offshore wave conditions are very similar at the eastern and western ends of the beach (Fig. 3), indicating that the differences in hydrodynamic conditions between these two zones are more likely to be found in the complex nearshore zone. This is one of the interests and essential challenges in understanding and modeling coastal processes

at Vougot beach and other sites with complex nearshore bathymetries (e.g. nearshore reefs at Narrabeen-Collaroy Beach).

*5.3. Significant depletion of sediment on the eastern part of the tidal beach*

Since the beginning of the surveys at Vougot beach, chronic erosion at the eastern end has led to the disappearance of beach sand exposing the underlying pebbles, cobbles, interglacial deposits and peat, especially on the intertidal beach (Fig. 12). The cores taken along this part of the beach (see principally profiles 1, 2, and 3) show that the thickness of available sand that is transported along the beach profile is essentially concentrated along the upper beach (~70 to 80 m from the dune toe) (Fig. 12a,b,c). Beyond this limit, the beach profile reaches a hard boundary layer, consisting mainly of Holocene peat, and/or Pleistocene silt and accumulation of a thin layer of coarse pebbles (Fig. 12e,f). The depletion of the sand stock of the intertidal beach can be explained by the regeneration of the dune after erosive episodes (e.g., the storm Johanna of March 10, 2008 or the storms of the winter 2013-2014) (Suanez et al., 2012). In the months following these erosive episodes, aeolian sediment transfers from the intertidal beach to the upper beach/dune rebuild the dune. However, these losses from the intertidal zone are not compensated for by a sediment source. Consequently, it is possible to hypothesize that in a few decades the regeneration processes of the dune/upper beach system will no longer act as efficiently, potentially leading to dune breaching, threatening to flood the low-lying zone currently protected by the dune. The erosion and/or breaching of barriers in Brittany due to sediment depletion has already been observed in some other coastal study cases (Stéphan et al., 2018b; Suanez et al., 2018a).

*5.4. Dune morphological change feedbacks on runup and EWL*

The observed morphological changes resulted mainly in a lowering of the beach profile (see Fig. 4), which impacts wave runup and consequently, *EWL*. The beach slope tan$\beta$ increases throughout the observation period (+55% trend in 17 years). By feedback, this increase contributes to the increase in wave runup height (+65%) (Fig. 8b) and *EWL* (+17%) (Fig. 8c), thus increasing the likelihood of further dune erosion. It is hypothesized that since 2004, the progressive lowering of the beach profile and steepening of the upper beach and lower dune has favored an increasingly frequent attack of the dune by *EWL*. Changes in the morphological conditions have led to an increase in wave runup and *EWL*, contributing to the maximum shoreline retreat of up to –20 m in the eastern part of the beach over the last two decades (see Fig. 10).

Searching for a quantitative relationship between the dune toe exceedance and sediment budget changes is complicated by the monthly survey frequency that includes periods of both erosion and accretion, and integral parameters do not take into account the sequence of events. For example, if a dune erosion episode occurs immediately following a survey, followed by dune regeneration, the resultant dune morphology is unlikely to be the same if a dune accretion phase was followed by an erosion episode (List et al., 2006). A second difficulty is properly accounting for the differences in sediment transport rates associated with dune erosion (assumed to be caused by hydrodynamical processes related to *EWL*) and dune accretion (assumed to be dominated by aeolian transport processes, which thus depends on the wind forcing and sediment humidity).

*5.5. Storm event frequency/intensity and dune erosion*

Long-term, high-frequency beach profile surveys are necessary to describe morphological changes, especially those related to the longer term impacts of storm events (Tsuchiya et al., 1982; Thom et al., 1991; Larson and Krauss, 1994; Lacey and Peck, 1998; McLean and Shen, 2006; Reeve et al., 2007; Kroon et al., 2008; Karunarathna et al., 2015; Masselink et al., 2016; Banno et al., 2020; Castelle et al., 2020; Bertin et al., 2022; Nicolae Lerma et al., 2022). At Vougot beach, significant *EWL* events that exceed the dune toe elevation and cause dune erosion show significant annual variability due to wave conditions (including wave runup) and tide levels, as well as the pre-storm morphology (i.e. dune toe elevation). During the 17-year survey period, the highest frequency of dune toe exceedance for all ($\Delta z_{exceedance} > 0$) and significant ($\Delta z_{exceedance} > 0.8$) events (Fig. 13) is observed during the first five years (2004-2008), when the dune toe elevation was at a minimum (Fig. 8c). Between 2009 and 2013, the number of dune toe exceedance events decreased significantly due to less energetic waves and a steady increase in the dune toe elevation after the Johanna storm event (Suanez et al., 2012). Then, the energetic winter storms of 2013-2014 caused a decrease in the dune toe elevation, leading to an increase in dune toe exceedance events. Since 2014, the dune has been in a progressive recovery phase (i.e., increase in the dune toe elevation), again decreasing the dune toe exceedance frequency. The cycles in dune toe exceedance frequency are related to the recovery phases of the dune after significant erosion events.

Following the approach of Prado et al. (2022), the return periods of the *EWL* and dune toe exceedance ($\Delta z_{exceedance}$) were calculated since the impacts of the *EWL* on the dune depends on both of these parameters. A Gumbel distribution was fit to the annual maximum values for both parameters to estimate the 2, 5, 10, 25, and 50-year return periods (Fig. 14a,b). The 50-year return period is the longest return period that may be estimated with only 17 years of data.

At Vougot beach, the *EWL* with a 50-year return period is approximately 10.6 m (9.7-11.3 m, 95% confidence limits), nearing the maximum elevation of the current dune (Fig. 14a). In comparison, the most significant event during the survey period (Table 3) experienced an *EWL* of 9.6 m (i.e., Anne storm in February 2014), which corresponds to an *EWL* with a return period of approximately 9 years (Fig. 8c). Other significant storms (e.g., Johanna 03/2008, Christine 03/2014, Imogen 02/2016, Eleanor 01/2018) fall in the range of *EWLs* (Table 3) with return periods ranging from 3 to 6 years. The dune toe exceedance 50-year return period is estimated to be about 3.8 m (2.3-5.0 m, 95% confidence limits) (Fig. 14b). The highest $\Delta z_{exceedance}$ was also reached during the Anne storm, with a maximum of 3.0 m, corresponding to a return period of approximately 20 years (Fig. 14b). This analysis emphasizes the importance of evaluating not only the *EWL* return periods, but also the dune toe exceedance return periods, which include the effects of dune toe elevation changes.

Masselink et al. (2016) studied the morphological impacts of the extreme wave activity during the winter 2013-2014 (including the Anne storm), concluding that it was the most energetic winter along most of the Atlantic coast of Europe since at least 1948, based on the analysis of offshore wave data simulations from 1948 to 2015. The current study shows that an analysis of the coastal erosion induced by the combined hydrodynamic and morphological conditions (*EWL*, including wave runup, and dune toe morphology) can reduce the return period of such extreme events. Similarly, Blaise et al. (2015) showed that shoreline erosion observed in Brittany during the 2013-2014 winter was comparable to that observed during the stormy winter of 1989-1990 (McCallum and Norris, 1990), i.e., about 25 years ago.

To reduce the uncertainties associated with the estimation of the return period of *EWL* events inducing significant coastal erosion, longer time series of measurements are needed, as well as multi-parameter studies including the effects of the dune toe position. In addition, this

analysis assumes that the statistics of *EWL* and dune toe exceedance are stationary, and a more complete analysis should take into account the impacts of SLR and changes in the wave climate.

Surveys carried out on other sandy beaches and gravel barriers in Brittany show that the events causing the most significant dune erosion in this study have also been observed at many sites through shoreline erosion dynamics and/or landward barrier migration (Table 4). The winter of 2013-2014 had the most significant impacts on coastal morphology in Brittany during the nearly two decades of surveys. It was characterized by a cluster of storms (Matthews et al., 2014; Wadey et al., 2014) that impacted the entire Western European coast (Masselink et al., 2015, 2016; Castelle et al., 2015; Blaise et al., 2015; Autret et al., 2016), and showed a similar frequency of storm events as the winter of 1989-1990 (McCallum and Norris, 1990; Betts et al., 2004). The wave heights recorded at the Pierres Noires buoy (Fig. 1) during the winter of 2013-2014 reached 12.3 to 12.4 m of $H_{sig}$ during the Petra storm of February, 5 and Ulla storm of February 14, respectively, with a $H_{max}$ of 23.5 m during the Petra storm of February 5, 2014 (Blaise et al., 2015).

## 6. Conclusion

This study showed that high frequency, medium to long-term beach surveys are an essential tool for improving knowledge of morphosedimentary and hydrodynamic processes. At Vougot beach, 17 years of monthly surveys show that the eastern end of the beach/dune system lost a significant volume of sediment, in agreement with the evolution of this part of the beach in recent decades since the construction of the Curnic jetty. The eroded sediment appears to have been transported to the western end of the beach, which showed substantial sediment gain. Longshore sediment transport from east to west is causing a beach rotation phenomenon related to the depletion of sediment supplies in the east. Hypotheses on the dynamics at the origin of this sedimentary transport are proposed, but need to be confirmed by field measurements.

As one would expect, the long-term trends in dune erosion or accretion are the result of phases of dune recovery and episodic significant erosion events. The evaluation of these episodic events based on the extreme water levels (*EWL*) exceeding the dune toe elevation ($\Delta z_{exceedance}$) shows a moderate correlation with the dune volume changes ($R^2 = 0.55$). This is mainly due to the complexities and nonlinearities in dune erosion and accretion processes, related to the hydrodynamic impacts (e.g., waves and water levels), and also the morphological characteristics (e.g., pre-storm morphology *via* the dune toe elevation). Completing weekly or more frequent surveys would improve understanding of these morphosedimentary processes although this approach would remain ambitious and extremely difficult to achieve. Nethertheless, the method implemented in this study made it possible to identify the storm events that generated significant erosion at Vougot beach and that have also been observed throughout North Brittany during the last 17 years.

## Acknowledgements

The beach surveys at Vougot beach were supported by the « *Institut National des Sciences de l'Univers* » (INSU-CNRS) in the framework of the French « *Service National d'Observation* » (SNO-DYNALIT). It is funded by the municipality of Guissény and the Regional Council of Brittany as a part of the « *Contrat Nature* » project. This study has also benefited from the Labex-Mer (ANR-10-LABX-0019) between 2011 and 2018, and from the ISblue program, Interdisciplinary graduate school for the blue planet (ANR-17-EURE-0015), since 2019. Both

of these programs were co-funded by a grant from the French government under the program "*Investissements d'Avenir*" embedded in France 2030.

**Bibliography**

Accensi, M., Alday Gonzalez, M.F., Maisondieu, C., Raillard, N., Darbynian, D., Old, C., Sellar, B., Thilleul, O., Perignon, Y., Payne, G., O'Boyle, L., Fernandez, L., Dias F., Chumbinho, R., Guitton, G., 2021. ResourceCODE framework: A high-resolution wave parameter dataset for the European Shelf and analysis toolbox. *Proceedings of the 14th European Wave and Tidal Energy Conference* 5-9th Sept 2021, Plymouth, UK. ISSN: 2706-6940 (online) 2706–6932, (CD-ROM) 2706–6932, (Print) 2182-1–2182-9. https://archimer.ifremer.fr/ doc/00736/84812/

Accensi, M., 2022. RESOURCECODE. IFREMER. https://doi.org/10.12770/d089a801-c853-49bd-9064-dde5808ff8d8

Almar, R., Castelle, B., Ruessink, B.G., Sénéchal, N., Bonneton, P., Marieu, V., 2010. Two- and three-dimensional double-sandbar system behaviour under intense wave forcing and a meso–macro tidal range. *Continental Shelf Research*, 30(7), 781–792. https://doi.org/10.1016/j.csr.2010.02.001

Autret, R., Dodet, G., Fichaut, B., Suanez, S., David, L., Leckler, F., Ardhuin, F., Ammann, J., Grandjean, P., Allemand, P., Filipot, J.-F., 2016. A comprehensive hydro-geomorphic study of cliff-top storm deposits on Banneg Island during winter 2013-2014. *Marine Geology*, 382, 37-55. https://doi.org/10.1016/j.margeo.2016.09.014

Battjes, J.A., 1974. *Surf similarity*. Proceedings of the 14th International Conference on Coastal Engineering ASCE, Copenhagen (Denmark), 24-28 June 1974, 466–480.

Banno, M., Nakamura, S., Kosuko, T., Nakagawa, Y., Yanagishima, S.-I., Kuriyama, Y., 2020. Long-term observations of beach variability at Hasaki, Japan. *Journal of Marine Science and Engineering*, 8(11), 871. https://doi.org/10.3390/jmse8110871

Banno, M., Kuriyama, Y., 2020. Supermoon drives beach morphological changes in the swash zone. *Geophysical Research Letters*, 47, e2020GL089745. https://doi.org/10.1029/2020GL089745

Banno M (2023). What can long-term in situ monitoring data tell us about our coastlines? *Cambridge Prisms: Coastal Futures*, 1(e8), 1–7. https://doi.org/10.1017/cft.2022.9

Barnard, P., Short, A., Harley, M., Splinter, K.D., Vitousek, S., Turner, I.L., Allan, J., Banno, M., Bryan, K.R., Doria, A., Hansen, J.E., Kato S., Kuriyama, Y., Randall-Goodwin, E., Ruggiero, P., Walker, I.J., Heathfield, D.K., 2015. Coastal vulnerability across the Pacific dominated by El Niño/Southern Oscillation. *Nature Geoscience*, 8, 801–807. https://doi.org/10.1038/ngeo2539

Battistini, R., 1954. Description du relief et des formations quaternaires du littoral breton entre L'aber Benoit et la baie de Goulven (Finistère). *Bulletin d'Information du Comité Central d'Océanographie et d'Etude des Côtes*, VI(3), 119–132.

Battistini, R., 1955. Description du relief et des formations quaternaires du littoral breton entre Brignogan et Saint-Pol-de-Léon (Finistère). *Bulletin d'Information du Comité Central d'Océanographie et d'Etude des Côtes*, VII(10), 468–493.

Battistini, R., Martin, S., 1956. La « Plate-forme à écueils » du Nord-Ouest de la Bretagne. *Norois*, 10, 147–161. https://doi.org/10.3406/noroi.1956.1121

Bertin, S., Floc'h, F., Le Dantec, N., Jaud, M., Cancouët, R., Franzetti, M., Cuq, V., Prunier, C., Ammann, J., Augereau, E., Lamarche, S., Belleney, D., Rouan, M., David, L., Deschamps, A., Delacourt, C., Suanez, S., 2022. A long-term dataset of topography and nearshore bathymetry at the macrotidal pocket beach of Porsmilin, France. *Scientific Data*, 9(79). https://doi.org/10.1038/s41597-022-01170-3

Betts, N.L., Orford, J.D., White, D., Graham, C.J., 2004. Storminess and surges in the South-Western Approaches of the eastern North Atlantic: the synoptic climatology of recent extreme coastal storms. *Marine Geology*, 210, 227–246. https://doi.org/10.1016/j.margeo.2004.05.010

Birkemeier, W., 1985. Field data on seaward limit of profile change. *Journal of Waterway, Port, Coastal and Ocean Engineering*, 111(3), 598–602. https://doi.org/10.1061/(ASCE)0733-950X(1985)111:3(598)

Bishop, C.T., Donelan, M.A., 1987. Measuring waves with pressure transducers. *Coastal Engineering*, 11(4), 309–328. https://doi.org/10.1016/0378-3839(87)90031-7

Blaise, E., Suanez, S., Stéphan, P., Fichaut, F., David, L., Cuq, V., Autret, R., Houron, J., Rouan, M., Floc'h, F., Ardhuin, F., Cancouët, R., Davidson, R., Costa, S., Delacourt, C., 2015. Bilan des tempêtes de l'hiver 2013-2014 sur la dynamique de recul du trait de côte en Bretagne. *Géomorphologie : Relief, Processus, Environnement*, 21(3), 267–292. https://doi.org/10.4000/geomorphologie.11104

Boak, E.H., Turner, I.L., 2005. Shoreline definition and detection: A review. *Journal of Coastal Research*, 21(4), 688–703. https://www.jstor.org/stable/4299462

Callaghan, D.P., Nielsen, P., Short, A.D., Ranasinghe, R., 2008. Statistical simulation of wave climate and extreme beach erosion. *Coastal Engineering*, 55(5), 375–390. https://doi.org/10.1016/j.coastaleng.2007.12.003

Callaghan, D.P., Ranasinghe, R., Short, A.D., 2009. Quantifying the storm erosion hazard for coastal planning. *Coastal Engineering*, 56(1), 90–93. https://doi.org/10.1016/j.coastaleng.2008.10.003

Cariolet, J.-M., Suanez, S., 2013. Runup estimations on macrotidal sandy beach. *Coastal Engineering*, 74, 11–218. https://doi.org/10.1016/j.coastaleng.2012.11.008

Carter, R.G. W., Hesp, P.A., Nordstrom, K.F., 1990. Erosional landforms in coastal dunes, in: Nordstrom, K., Psuty, N., Carter, B. (Eds.), Coastal dunes. Form and process. John Wiley & Sons, England, pp. 217–250.

Castelle, B., Bonneton, P., Dupuis, H., Sénéchal, N., 2007. Double bar beach dynamics on the high-energy meso-macrotidal French Aquitanian Coast: A review. *Marine Geology*, 245(1-4), 141–159. https://doi.org/10.1016/j.margeo.2007.06.001

Castelle, B., Ruessink, B.G., Bonneton, P., Bruneau, N., Marieu, V., 2008. Modeling of coupled and noncoupled behavior of a double sandbar system: self-organization and morphological forcing. Proceedings of the 31st International Conference « Coastal Engineering 2008 », Hamburg, Germany, May 2009, 2003–2014. https://doi.org/10.1142/9789814277426_0165

Castelle, B., Ruessink, B.G., 2011. Modeling formation and subsequent nonlinear evolution of rip channels: Time-varying versus time-invariant wave forcing. *Journal of Geophysical Research*, 116(F4), F04008. https://doi.org/10.1029/2011JF001997

Castelle, B., Marieu, V., Bujan, S., Splinter, K.D., Robinet, A., Sénéchal, N., Ferreira, S., 2015. Impact of the winter 2013–2014 series of severe Western Europe storms on a double-barred sandy coast: Beach and dune erosion and megacusp embayments. *Geomorphology*, 238, 135–148. https://doi.org/10.1016/j.geomorph.2015.03.006

Castelle, B., Bujan, S., Marieu, V., Ferreira, S., 2020. 16 years of topographic surveys of rip-channelled high-energy meso-macrotidal sandy beach. *Scientific Data*, 7, 410. https://doi.org/10.1038/s41597-020-00750-5

Castelle, B., Bujan, S., Ferreira, S., Dodet, G., 2017. Foredune morphological changes and beach recovery from the extreme 2013/2014 winter at a high-energy sandy coast. *Marine Geology*, 385, 41–55. https://doi.org/10.1016/j.margeo.2016.12.006

Chataigner, T., 2021. Modélisation empirique de l'évolution des plages integrant les processus cross-shore et longshore. PhD thesis, ENPC, École doctorale Sciences, Ingénierie et Environnement, Marne-la-Vallée, France. http://www.theses.fr/2021ENPC0028

Davidson, M., Splinter, K., Turner, I., 2013. A simple equilibrium model for predicting shoreline change. *Coastal Engineering*, 73, 191–202. https://doi.org/10.1016/j.coastaleng.2012.11.002

Dehouck, A., Dupuis, H., Sénéchal, N., 2009. Pocket beach hydrodynamics: The example of four macrotidal beaches, Brittany, France. *Marine Geology*, 266, 1–17. https://doi.org/10.1016/j.margeo.2009.07.008

Didier, D., Caulet, C., Bandet, M., Bernatchez, P., Dumont, D., Augereau, E., Floc'h, F., Delacourt, C., 2020. Wave runup parameterization for sandy, gravel and platform beaches in a fetch-limited, large estuarine system. *Continental Shelf Research*, 192, 104024. https://doi.org/10.1016/j.csr.2019.104024

Dissanayake, P., Yates, M.L., Suanez, S., Floc'h, F., Krämer, K., 2021. Climate change impacts on coastal wave dynamics at Vougot beach, France. *Journal of Marine Science and Engineering*, 9, 1009. https://doi.org/10.3390/jmse9091009

Dodet, G., Castelle, B., Masselink, G., Scott, T., Davidson, M., Floc'h, F., Jackson, D., Suanez, S., 2019. Beach recovery from extreme storm activity during the 2013/14 winter

along the Atlantic coast of Europe. *Earth Surface Processes and Landforms*, 44(1), 393–401. https://doi.org/10.1002/esp.4500

Fichaut, B., Suanez, S., 2010. Dynamiques d'arrachement, de transport et de dépôt de blocs cyclopéens par les tempêtes. Exemple de la tempête du 10 mars 2008 sur l'île de Banneg (archipel de Molène, Finistère). *Norois*, 215, 33–58. https://doi.org/10.400/norois.3224

Fichaut, B., Suanez, S., 2011. Carrying, transport and deposition of cliff-top storm deposits during extreme event: Banneg Island, Brittany. Marine Geology, 283 (1-4), 36–55. https://doi.org/10.1016/j.margeo.2010.11.003

Fichaut, B., Stéphan, P., Suanez, S., Ammann, J., Grandjean, P., 2017. Rapport sur le suivi morphosédimentaire du sillon de Talbert pour l'année 2016, GEOMER - LETG UMR 6554 CNRS, I.U.E.M., 25p. https://www-iuem.univ-brest.fr/pops/attachments/1361

Floc'h, F., Le Dantec, N., Lemos, C., Cancouët, R., Sous, D., Petitjean, L., Bouchette, F., Ardhuin, F., Suanez, S., Delacourt, C., 2016. Morphological response of a macrotidal embayed beach, Porsmilin, France. *Journal of Coastal Research*, SI75, 373–377. http://dx.doi.org/10.2112/SI75-075.1

Gallop, S.L., Kennedy, D.M., Loureiro, C., Naylor, L.A., Muñoz-Pérez, J.J., Jackson, D.W.T., Fellowes, T.E., 2020. Geologically controlled sandy beaches: Their geomorphology, morphodynamics and classification. *Science of The Total Environment*, 731, 139123. https://doi.org/10.1016/j.scitotenv.2020.139123.

George, K.J., Simon, B., 1984. The species concordance method of tide prediction in estuaries. *The International Hydrographic Review*, LXI(1), 121–146. https://journals.lib.unb.ca/index.php/ihr/article/view/23515

Gorczyńska, A., Stéphan, P., Paller, Y., Nicolas, C., Penaud, A., David, O., Vidal, M., Le Gall, B., 2023. Holocene evolution of coastal dunes in western France: Regional reconstruction from archaeological and historical data. *Aeolian Research*, 60, 100851. https://doi.org/10.1016/j.aeolia.2022.100851

Guilcher, A., Hallégouët, B., 1991. Coastal dunes in Brittany and their management. *Journal of Coastal Research.* 7(2) 517–533. https://www.jstor.org/stable/4297859

Hanson, H., 1989. Genesis: A generalized shoreline change numerical model. *Journal of Coastal Research*, 5(1), 1–27. http://www.jstor.org/stable/4297483

Harley, M.D., Turner, I.L., Short, A.D., Ranasinghe, R., 2011a. Assessment and integration of conventional, RTK-GPS and image-derived beach survey methods for daily to decadal coastal monitoring. *Coastal Engineering*, 58(2), 194–205. https://doi.org/10.1016/j.coastaleng.2010.09.006

Harley, M.D., Turner, I.L., Short, A.D., Ranasinghe, R., 2011b. A reevaluation of coastal embayment rotation: The dominance of cross-shore versus alongshore sediment transport processes, Collaroy-Narrabeen Beach, southeast Australia. *Journal of Geophysical Research*, 116, F04033. https://doi.org/10.1029/2011JF001989

Hashimoto, H., Uda, T., 1982. Field investigation of beach profiles changes and the analysis using empirical eigenfunctions. *Coastal Engineering Proceedings*, 1(18), 84. https://doi.org/10.9753/icce.v18.84

Hillen, H., Roelse, P., 1995. Dynamic preservation of the coastline in the Netherlands. *Journal of Coastal Conservation*, 1(1), 17–28. https://www.jstor.org/stable/25098187

Holland, K.T., Holman, R.A., 1993. The statistical distribution of swash maxima on natural beaches. *Journal of Geophysical Research*, 98(C6), 10271–10278. https://doi.org/10.1029/93JC00035

Holman, R.A., 1986. Extreme value statistics for wave run-up on a natural beach. *Coastal Engineering*, 9(6), 527–544. https://doi.org/10.1016/0378-3839(86)90002-5

Holman, R.A., Sallenger, A.H., 1985. Setup and swash on a natural beach. *Journal of Geophysical Research*, 90(C1), 945– 953. https://doi.org/10.1029/JC090iC01p00945

Hom-ma, M., Horikawa, K., Komori, S., 1966. Response characteristics of underwater wave gauge. *Coastal Engineering in Japan*, 9(1), 45–54. https://doi.org/10.1080/05785634.1966.11924671

Howd, P.-A., Birkemeir, W.-A., 1987. Beach and nearshore survey data: 1981-1984, CERC Field Research Facility: Technical Report CERC-87-9. U.S. Army Waterways Experiment Station, Vicksburg, Mississippi, 139p.

Hunt, I.A., 1959. Design of seawalls and breakwaters. *Journal of the Waterways and Harbors Division*, 85(3), 123–152. https://doi.org/10.1061/JWHEAU.0000129

Huntley, D.A., Short, A.D., 1992. On the spacing between observed rip currents. *Coastal Engineering*, 17(3-4), 211–225. https://doi.org/10.1016/0378-3839(92)90052-V

Jaud, M., Delacourt, C., Le Dantec, N., Allemand, P., Ammann, J., Grandjean, P., Nouaille, H., Prunier, C., Cuq, V., Augereau, E., Cocquempot, L., Floc'h, F., 2019. Diachronic UAV photogrammetry of a sandy beach in Brittany (France) for a long-term coastal observatory. *ISPRS International Journal of Geo-Information*, 8, 267. https://doi.org/10.3390/ijgi8060267

Karunarathna, H.U., Mase, H., Baba, Y., 2015. Analysis of multi-scale morphodynamic behavior of a high energy beach facing the Sea of Japan. *Frontiers in Marine Science*, 2, 51. https://doi.org/10.3389/fmars.2015.00051

Kroon, A., Larson, M., Möller, I., Yokoki, H., Rozynski, G., Cox, J., Larroude, P., 2008. Statistical analysis of coastal morphological data sets over seasonal to decadal time scales. *Coastal Engineering*, 55(7-8), 581–600. https://doi.org/10.1016/j.coastaleng.2007.11.006

Koster, M.-J., Hillen, R., 1995. Combat erosion by law: coastal defence policy for The Netherlands. *Journal of Coastal Research*, 11(4), 1221–1228. https://www.jstor.org/stable/4298425

Lacey, E.M., Peck, J.A., 1998. Long-Term beach profile variations along the South Shore of Rhode Island, U.S.A. *Journal of Coastal Research*, 14(4), 1255–1264. http://www.jstor.org/stable/4298885

Larson, M., Kraus, N.C., 1994. Temporal and spatial scales of beach profile change, Duck, North Carolina. *Marine Geology*, 117(1-4), 75–94. https://doi.org/10.1016/0025-3227(94)90007-8.

Lee, G.-H., Birkemeir, W.-A., 1993. Beach and nearshore survey data: 1985-1991, CERC Field Research Facility: Technical Report CERC-93-3. U.S. Army Waterways Experiment Station, Vicksburg, Mississippi, 26p. + appendices.

Lemos, C., Floc'h, F., Yates, M., Le Dantec, N., Marieu, V., Hamon, K., Cuq, V., Suanez, S., Delacourt, C., 2018. Equilibrium modeling of the beach profile on a macrotidal embayed beach. *Ocean Dynamics*, 68(9), 1207–1220. https://doi.org/10.1007/s10236-018-1185-1

Lippmann, T.C., Holman, R.A., 1990. The spatial and temporal variability of sandbar morphology. *Journal of Geophysical Research*, 95(C7), 11575–11590. https://doi.org/10.1029/JC095iC07p11575

List, J.H., Farris, A.S., Sullivan, C. 2006. Reversing storm hotspots on sandy beaches: Spatial and temporal characteristics. *Marine Geology*, 226(3-4), 261–279, https://doi.org/10.1016/j.margeo.2005.10.003

Louisse, C.-J., van der Meulen, F., 1991. Future coastal defence in the Netherland: strategies for protection and sustainable development. *Journal of Coastal Research*, 7(4), 1027–1041. https://www.jstor.org/stable/4297923

Mahabot, M.-M., Jaud, M., Pennober, G., Le Dantec, N., Troadec, R., Suanez, S., Delacourt, C., 2017. The basics for a permanent observatory of shoreline evolution in tropical environments; lessons from back-reef beaches in La Reunion Island. *Comptes Rendus Geoscience*, 349, 330–340. https://doi.org/10.1016/j.crte.2017.09.010

Mason, C., 1985. Recent R&D accomplishments at the coastal engineering research center field research facility. OCEANS '85 - Ocean Engineering and the Environment, 78–84, https://doi.org/10.1109/OCEANS.1985.1160312

Masselink, G., Short, A.D., 1993. The effect of tide range on beach morphodynamics and morphology: a conceptual beach model. *Journal of Coastal Research*, 9(3), 785–800. https://www.jstor.org/stable/4298129

Masselink, G., Scott, T., Poate, T., Russell, P., Davidson, M., Conley, D., 2015. The extreme 2013/14 winter storms: hydrodynamic forcing and coastal response along the southwest coast of England. *Earth Surface Processes & Landforms*, 41, 378–391. https://doi.org/10.1002/esp.3836

Masselink, G., Castelle, B., Scott, T., Dodet, G., Suanez, S., Jackson, D., Floc'h, F., 2016. Extreme wave activity during 2013/14 winter and morphological impacts along the Atlantic coast of Europe. *Geophysical Research Letters*, 43(5), 2135–2143. https://doi.org/10.1002/2015GL067492

Matthews, T., Murphy, C., Wilby, R.L., Harrigan, S., 2014. Stormiest winter on record for Ireland and UK. *Nature Climate Change*, 4, 738–740. https://doi.org/10.1038/nclimate2336

McCallum, E., Norris, W.J.T., 1990. The storms of January and February 1990. *The Meteorological Magazine*, 119, 201–210.

McLean, R., Shen, J.-S., 2006. From foreshore to foredune: foredune development over the last 30 years at Moruya Beach, New South Wales, Australia. *Journal of Coastal Research*, 22(1), 28–36. https://doi.org/10.2112/05A-0003.1

Montaño, J., Coco, G., Chataigner, T., Yates, M., Le Dantec, N., Suanez, S., Cagigal, L., Floc'h, F., Townend, I., 2021. Time-scales of a dune-beach system and implications for shoreline modeling. *Journal of Geophysical Research: Earth Surface*, 126, e2021JF006169. https://doi.org/10.1029/2021JF006169

Moore, L.J. 2000. Shoreline Mapping Techniques. *Journal of Coastal Research*, 16(1), 111–124. http://www.jstor.org/stable/4300016

Nicholls, R.J., Birkemeier, W.A., Lee, G., 1998. Evaluation of depth of closure using data from Duck, NC, USA. *Marine Geology*, 148(3-4), 179–201. https://doi.org/10.1016/S0025-3227(98)00011-5

Nicolae Lerma, A., Castelle, B., Marieu, V., Robinet, A., Bulteau, T., Bernon, N., Mallet, C., 2022. Decadal beach-dune profile monitoring along a 230-km high-energy sandy coast: Aquitaine, southwest France. *Applied Geography*, 139, 102645. https://doi.org/10.1016/j.apgeog.2022.102645

Ostrowski, R., Schönhofer, J., Szmytkiewicz, P. 2016. South Baltic representative coastal field surveys, including monitoring at the Coastal Research Station in Lubiatowo, Poland. *Journal of Marine Systems*, 162, 89-97. https://doi.org/10.1016/j.jmarsys.2015.10.006.

Pape, L., Kuriyama, Y., Ruessink, B.G., 2010. Models and scales for cross-shore sandbar migration, *Journal of Geophysical Research*, 115, F03043. https://doi.org/10.1029/2009JF001644

Pianca, C., Holman, R., Siegle, E., 2015. Shoreline variability from days to decades: Results of long-term video imaging, *Journal of Geophysical Research*, 120(3), 2159–2178, https://doi.org/10.1002/2014JC010329

Prado, M.F.V., Dalinghaus, C., Gomes da Silva, P., Weschenfelder, J., Klein, A.H.F., 2022. Estimating the different return periods of storm impact regimes on beach and foredune systems based in hindcast data: Applications to exposed and sheltered beaches of Santa Catarina Island, Brazil. *Journal of Coastal Research*, 38(4), 844–859. https://doi.org/10.2112/JCOASTRES-D-17-00123.1

Quartel, S., Kroon, A., Ruessink, B.G., 2008. Seasonal accretion and erosion patterns of a microtidal sandy beach. *Marine Geology*, 250(1-2), 19–33. https://doi.org/10.1016/j.margeo.2007.11.003

Ranasinghe, R., McLoughlin, R., Short, A.D., Symonds, G., 2004. The Southern Oscillation Index, wave climate and beach rotation. *Marine Geology*, 204(3-4), 273–287. https://doi.org/10.1016/S0025-3227(04)00002-7

Reeve, D., Li, Y., Lark, M., Simmonds, D., 2007. An investigation of the multi-scale temporal variability of beach profiles at Duck using wavelet pasket transforms. *Coastal Engineering*, 54(5), 401–415. https://doi.org/10.1016/j.coastaleng.2006.11.008

REFMAR, 2019. REFMAR.Shom.fr, Réseaux marégraphiques français. http://refmar.shom.fr/fr/donnees-refmar-sur-data.shom.fr/acces-aux-donnees

Ruessink, B.G., Wijnberg, K.M., Holman, R.A., Kuriyama, Y., van Enckevort, I.M.J., 2003. Intersite comparison of interannual nearshore bar behavior. *Journal of Geophysical Research*, 108(C8), 3249. https://doi.org/10.1029/2002JC0015

Ruessink, B.G., Kuriyama, Y., Reniers, A.J.H.M., Roelvink, J.A., Walstra, D.J.R., 2007. Modeling cross-shore sandbar behavior on the timescale of weeks, *Journal of Geophysical Research*, 112, F03010. https://doi.org/10.1029/2006JF000730.

Ruggiero, P., Voigt, B., Kaminsky, G., 2000. Beach monitoring for enhanced decision-making. Proceeding of the 17th Conference of the Coastal Society « Coasts at the Millennium », 9-12 July 2000, Portland, Oregon USA. https://nsgl.gso.uri.edu/oresu/oresuc00002/pdffiles/papers/087.pdf

Ruggiero, P., Komar, P.D., McDouglas, W.G., Marra, J.J., Beach, R.A., 2001. Wave runup, extreme water levels and the erosion properties backing beaches. *Journal of Coastal Research*, 17(2), 407–419. https://www.jstor.org/stable/4300192

Sallenger, A.H., Holman, R.A., Birkemeier, W.A., 1985. Storm-induced response of e nearshore-bar system. *Marine Geology*, 64(3-4), 237–257. https://doi.org/10.1016/0025-3227(85)90107-0

SHOM, 2008. LITTO3D®
https://services.data.shom.fr/geonetwork/srv/api/records/BATHYMETRIE_L3D.xml

Short, A.D., Hogan, C.L., 1994. Rips and beach hazards, their impact on public safety and implications for coastal management. *Journal of Coastal Research* SI12, 197–209. https://www.jstor.org/stable/25735599

Short, A., Trenbanis, A.C., 2004. Decadal scale patterns in beach oscillation and rotation Narrabeen Beach, Australia time series, PCA and wavelet analysis. *Journal of Coastal Research*, 20(2), 523–532. https://www.jstor.org/stable/4299308

Short, A.D., Bracs, M.A., Turner, I.L., 2014, Beach oscillation and rotation: local and regional response on three beaches in southeast Australia. *Journal of Coastal Reserch,* 70(SI), 712–717. https//doi.org/10.2112/SI-120.1

Simon, B., Gonella, J., Manley, D., Shipman, S., 2013. Coastal Tides. Second edition, Eds. Institut Océanographique, 409p.

Southgate, H.-N., 2008. Data-based forecasting of beach volumes on monthly to yearly timescales. *Coastal Engineering*, 55(12), 1005–1015. https://doi.org/10.1016/j.coastaleng.2008.03.016

Stéphan, P., Suanez, S., Fichaut, B., 2010. Franchissement et recul des cordons de galets par rollover. Impact de la tempête du 10 mars 2008 dans l'évolution récente du Sillon de Talbert (Côtes d'Armor, Bretagne). *Norois*, 215, 59–75. https://doi.org/10.4000/norois.3252

Stéphan, P., Suanez, S., Fichaut, B., 2012. Long-term morphodynamic evolution of the Sillon de Talbert gravel barrier (Brittany, France). *Shore & Beach*, 80(1), 19–36.

Stéphan, P., Suanez, S., Fichaut, B., Autret, R., 2017. Evolution morpho-sédimentaire du littoral de l'archipel, in: Ehrhold, A., Le Gall, B. (Eds.), Atlas de l'archipel de Molène. Géologie, géomorphologie et sédimentologie. Editions Quae, Versailles, pp. 81–98.

Stéphan, P., Dodet, G., Tardieu, I., Suanez, S., David, L., 2018a. Dynamique pluri-décennale du trait de côte en lien avec les variations des forçages météo-océaniques au nord de la Bretagne (baie de Goulven, France). *Géomorphologie : Relief, Processus, Environnement*, 24(1), 79–102. https://doi.org/10.4000/geomorphologie.11908

Stéphan, P., Suanez, S., Fichaut, B., Autret, R., Blaise, E., Houron, J., Ammann, J., Grandjean, P., 2018b. Monitoring the medium-term retreat of a gravel spit barrier and management strategies, Sillon de Talbert (North Brittany, France). *Ocean & Coastal Management*, 158, 64–82. https://doi.org/10.1016/j.ocecoaman.2018.03.030

Stéphan, P., Suanez, S., Houron, J., Ammann, J., Fichaut, B. 2018c. Suivi pluri-décennal de la flèche de galets du Sillon de Talbert (Pleubian, Côtes d'Armor) à partir de modèles numériques de terrain (MNT). INDIGEO [dataset]. https://doi.org/10.35110/8e37c01f-4cec-4edb-8c01-7047725f7dc4

Stéphan, P., Blaise, E., Suanez, S., Fichaut, B., Autret, R., Floc'h, F., Cuq, V., Le Dantec, N., Ammann, J., David, L., Jaud, M., Delacourt, C., 2019a. Long to medium to short-term shoreline dynamics of the Brittany coast (Western France). *Journal of Coastal Research*, SI88, 89–109. https://doi.org/10.2112/SI88-008.1

Stéphan, P., Fichaut, B., Suanez, S., Ammann, J., Tardieu, I., James, D., Mury, A., Houron, J., 2019b. Rapport sur le suivi morphosédimentaire du sillon de Talbert pour l'année 2018, LETG-Brest UMR 6554 CNRS, I.U.E.M., 100p. (avec annexes). https://www-iuem.univ-brest.fr/pops/attachments/2138

Stéphan, P., Fichaut, B., Suanez, S., Ammann, J., Houron, J., 2020. Rapport sur le suivi morphosédimentaire du sillon de Talbert pour l'année 2020, LETG-Brest UMR 6554 CNRS, I.U.E.M., 22p. (avec annexes). https://www-iuem.univ-brest.fr/pops/attachments/2296

Stockdon, H.F., Holman, R.A., Howd, P.A., Sallenger, A.H., 2006. Empirical parameterization of setup, swash, and runup. *Coastal Engineering*, 53(7), 573–588. https://doi.org/10.1016/j.coastaleng.2005.12.005

Suanez, S., Cariolet, J.-M., Fichaut, B., 2010a. Monitoring of Recent Morphological Changes of the Dune of Vougot Beach (Brittany, France) Using Differential GPS. *Shore & Beach,* 78(1), 37–47.

Suanez, S., Cariolet, J.-M., 2010b. L'action des tempêtes sur l'érosion des dunes : les enseignements de la tempête du 10 mars 2008. *Norois,* 215, 77–99. https://doi.org/10.400/norois.3212

Suanez, S., Stéphan, P., 2011. Effects of Natural and Human Forcing on Mesoscale Shoreline Dynamics of Saint-Michel-en-Grève Bay (Brittany, France). *Shore & Beach,* 79(2), 19–38.

Suanez, S., Fichaut, B., Magne, R., Ardhuin, F., Corman, D., Stéphan, P., Cariolet, J.-M., 2011. Changements morphologiques et bilan sédimentaire des formes fuyantes en queue de comète de l'archipel de Molène (Bretagne, France). *Géomorphologie : Relief, Processus, Environnement,* 11(2), 187–204. https://doi.org/10.4000/geomorphologie.9397

Suanez, S., Cariolet, J.-M., Cancouët, R., Ardhuin, F., Delacourt, C., 2012. Dune recovery after storm erosion on a high-energy beach: Vougot beach, Brittany (France). *Geomorphology,* 139–140, 16-33. https://doi.org/10.1016/j.geomorph.2011.10.014

Suanez, S., Cancouët, R., Floc'h, F., Blaise, E., Ardhuin, F., Filipot, J.-F., Cariolet, J.-M., Delacourt, C., 2015. Observations and predictions of wave runup, extreme water levels, and medium-term dune erosion during storm conditions. *Journal of Marine Science and Engineering,* 3 (3), 674–698. https://doi.org/10.3390/jmse3030674

Suanez, S., Blaise, E., Cariolet, J.-M., David, L., 2016a. Donnees pluri-décennales de suivi de profils de la plage/dune du Vougot à Guissény (Finistere, France). INDIGEO [dataset]. https://doi.org/10.35110/c120a3fe-9f54-45b3-b58b-1be6ba1deb99

Suanez, S., Fichaut, B., Blaise, E., Cariolet, J.-M., David, L. 2016b. Suivi pluri-décennal de la plage/dune du Vougot (Guissény, Finistère) à partir de modèles numériques de terrain (MNT). INDIGEO [dataset]. https://doi.org/10.35110/678d7660-43fd-49b7-9a01-3b1c2f822914

Suanez, S., Blaise, E. 2016. Données de suivi pluriannuel du trait de côte de la plage du Vougot (Guissény, Finistère). INDIGEO [dataset]. https://doi.org/10.35110/b59f2a81-f005-4657-a497-cf969b74e332

Suanez, S., Blaise, E., Ammann, J., Grandjean, P., 2017. Rapport sur le suivi morphosédimentaire du cordon dunaire de la plage du Vougot pour l'année 2016, GEOMER - LETG UMR 6554 CNRS, I.U.E.M., 18p. https://www-iuem.univ-brest.fr/pops/attachments/1336

Suanez, S., Floc'h, F., 2018. Mesures des conditions hydrodynamiques côtières sur la plage du Vougot (Guissény, Finsitère). INDIGEO [dataset]. https://doi.org/10.35110/4dba3ab7-0ea0-4a61-b1d7-8a134f3b4f57

Suanez, S., Stéphan, P., Floc'h, F., Autret, R., Fichaut, B., Blaise, E., Houron, J., Ammann, J., Grandjean, P., Accensi, M., André, G., Ardhuin, F., 2018a. Fifteen years of hydrodynamic forcing and morphological changes leading to breaching of a gravel spit, Sillon de Talbert

(Brittany). *Géomorphologie : Relief, Processus, Environnement*, 24(4), 403–428. https://doi.org/10.4000/geomorphologie.12677

Suanez, S., Stéphan, P., Houron, J. 2018b. Données du suivi mensuel de profils de plage de la flèche de galets du Sillon de Talbert (Pleubian, Bretagne nord). INDIGEO [dataset]. https://doi.org/10.35110/5000bf97-652e-4cef-863e-572d0cbceac3

Suanez, S., 2019. Rapport sur le suivi morphosédimentaire du cordon dunaire de la plage du Vougot pour l'année 2018, LETG-Brest UMR 6554 CNRS, I.U.E.M., 16p. https://www-iuem.univ-brest.fr/pops/attachments/2159

Suanez, S., 2021. Rapport sur le suivi morphosédimentaire du cordon dunaire de la plage du Vougot pour l'année 2020, LETG-Brest UMR 6554 CNRS, I.U.E.M., 16p. https://www-iuem.univ-brest.fr/pops/attachments/2318

Suanez, S., Stéphan, P., Autret, R., Houron, J., Floc'h, F., Davic, L., Ammann, J., Accensi, M., André, G., Le Guyader, D., Cancouët, R., 2022. Catastrophic overwash and rapid retreat of the gravel spit barrier during storm events (Sillon de Talbert, North Brittany, France). *Earth Surface Processes and Landforms*, 47(8), 2014–2043. https://doi.org/10.1002/esp.5361

Tamura, T., Oliver, T.S.N., Cunningham, A.C., Woodroffe, C.D. 2019. Recurrence of extreme coastal erosion in SE Australia beyond historical timescales inferred from beach ridge morphostratigraphy. *Geophysical Research Letters*, 46, 4705–4714. https://doi.org/10.1029/2019GL083061

Thom, B., Hall, W., 1991. Behaviour of beach profiles during accretion and erosion dominated periods. *Earth Surface Processes and Landforms*, 16(2), 113–127. https://doi.org/10.1002/esp.3290160203

Tsuchiya, Y., Shirai, T., Yamashita, T., 1982. Long-term changes in beach profiles at Ogata Coast. *Bulletin of the Disaster Prevention Research Institut*, 32(3-292), 171–187. http://hdl.handle.net/2433/124311

Tucker, M.J., Pitt, E.G., 2001. Waves in Ocean Engineering. Elsevier Science Ltd, 548p.

Turner, I.L., Harley, M., Short, A.D., Simmons, J.A., Bracs, M.A., Phillips, M.S., Splinter, K.D., 2016. A multi-decade dataset of monthly beach profile surveys and inshore wave forcing at Narrabeen, Australia. *Scientific Data*, 3, 160024. https://doi.org/10.1038/sdata.2016.24

Wadey, M.P., Haigh, I.D., Brown, J.M., 2014. A century of sea level data and the UK's 2013/14 storm surges: an assessment of extremes and clustering using the Newlyn tide gauge record. *Ocean Science Discussions*, 11(4), 1995–2028. https://doi.org/10.5194/osd-11-1995-2014

Wijnberg, K.M., Terwindt, J.H.J., 1995. Extracting decadal morphological behaviour from high-resolution, long-term bathymetric surveys along the Holland coast using eigenfunction analysis. *Marine Geology*, 126(1-4), 301–330. https://doi.org/10.1016/0025-3227(95)00084-C

Wright, L.D., Short, A.D., 1984. Morphodynamic variability of surf zones and beaches: A synthesis. *Marine Geology*, 56(1-4), 93–118. https://doi.org/10.1016/0025-3227(84)90008-2

Wright, L.D., Short, A.D., Boon III, J.D., Hayden, B., Kimball, S., List, J.H., 1987. The morphodynamic effects of incident wave groupiness and tide range on an energetic beach. *Marine Geology*, 74(1-2), 1–20. https://doi.org/10.1016/0025-3227(87)90002-8

WW3DG (The WAVEWATCH III ® Development Group), 2019. User manual and system documentation of WAVEWATCH III® version 6.07. Tech. Note 333, NOAA/NWS/NCEP/MMAB, College Park, MD, USA, 465p. + Appendices.

Yates, M.L., Guza, R.T., O'Reilly, W.C., 2009. Equilibrium shoreline response: Observations and modeling. *Journal of Geophysical Research*, 114(C9), C09014. https://doi.org/10.1029/2009JC005359

Zhang, J., Larson, M., 2021. Decadal-scale subaerial beach and dune evolution at Duck, North Carolina. *Marine Geology*, 440, 106576, https://doi.org/10.1016/j.margeo.2021.106576

**Fig. 1.** Location maps. a) Regional scale. b) Local scale. c) Zoom of Vougot beach showing the location of the 6 transects of beach profile measurements. DEMs used for (a) and (b) are from the *Service Hydrographique et Océanographique de la Marine* database Litto3D® (SHOM, 2008). The wave rose in (a) was calculated from data obtained in 64 m depth (4°50'10''W and 48°44'30''N) by running the TOMAWAC spectral wave model over the period 1979–2002 (source: *Laboratoire National d'Hydraulique et d'Environnement, LNHE-EDF Chatou, and Centre d'Etudes Techniques Maritimes et Fluviales, CETMEF-Brest*) (after Suanez et al. 2012). d) Aerial photography taken on August 8, 2012 (source: E. Le Cornec, GeosAEL) showing the comet tails observed behind the small inlets or reefs located in front of the beach.

**Fig. 2.** Schematics of the beach-dune profile analysis at a given transect. a) Beach/dune profile compartments. b) Method of calculating the eroded and accumulated sediment volumes along the profile between two dates $t_i$ and $t_{i+1}$.

**Fig. 3.** Comparison of the hindcast offshore wave characteristics (left column) and the differences (right column) between the nodes located at the eastern (node 138362) and western (node 138170) extremities of the nearshore zone (see figure 1c for the point locations): (a, b) significant wave height $H_{m0}$, (c, d) mean period $T_{m-1,0}$, and (e, f) mean direction $\theta$.

**Fig. 4.** Envelopes (shaded gray) of cross-shore profiles showing the first and the last beach/dune profile measurements and the amplitude of morphological variability as a function of distance cross-shore, characterized by the standard deviation of elevation for profiles 1 to 6.

**Fig. 5.** Maximum and minimum profiles and the difference (profile max – profile min) calculated from the envelope of the profiles for the whole survey period illustrating the magnitude of elevation changes along the beach/dune profile.

**Fig. 6.** Evolution of the sediment budget of the beach/dune system (a) and the dune *sticto sensu* (b), as defined in section 3.2. (Tab. 1). The green bars correspond to the measured sediment budget changes between the high frequency surveys, and the red line corresponds to the cumulated sediment budget changes.

**Fig. 7.** Time series of the (a) significant wave height, (b) wave energy flux and (c) significant wave height and water level. The horizontal lines in (a) and (b) show the thresholds for wave events exceeding the 99.9% quantile $H_{m0}$ = 6.7 m (orange circles in (a) and (b)), and a wave energy flux corresponding to the 99.9% quantile $H_{m0}$ and T=15.5 s (magenta circles in (b)), respectively. The horizontal dashed lines in panel (c) indicate the 97% thresholds for the significant wave height $H_{m0}$ =4.2 m (blue) and high tide water level $WL_{HT}$ = 4.4 m (green), and the vertical red lines indicate the dates for which both the $H_{m0}$ and $WL_{HT}$ exceed the 97% thresholds.

**Fig. 8.** Time series at profile 1 of the (a) beach slope and (b) estimated runup (Eq. 10) calculated from the most recent profile, and (c) extreme water level (*EWL*) and dune toe position, identifying approximately 150 events when the *EWL* estimate exceeded the dune toe elevation. The dashed lines show the linear regression over the 17-year time period. (d) Amplitude of the dune toe exceedance $\Delta z_{exceedance}$ and magnitude of the dune sediment budget changes. The solid blue line and shaded area represent the mean ($\bar{x}\Delta z_{exceedance}$) and standard deviation ($\sigma\Delta z_{exceedance}$) between subsequent beach profile surveys. The vertical gray bars indicate time periods showing significant potential for erosion, with $\Delta z_{exceedance}$ values larger than the mean plus 0.5 times the standard deviation (0.8 m).

**Fig. 9.** Probability density (a) and cumulative density (b) distributions of the dune toe exceedance during the survey period (bars), and by distinguishing time periods where the sediment budget was in an erosive (red line) or accretive (blue line) phase.

**Fig. 10.** Shoreline position on 2000 June, 16 (red) and 2021 July, 06 (blue) (a). DEM is from the *Service Hydrographique et Océanographique de la Marine* database Litto3D® (SHOM, 2008). (b) Quantification of shoreline changes (erosion/progradation in meters) as a function of the transect number indicated in box (c). Transects #1 to 36 in (c) were automatically generated by DSAS-based processing (Digital Shoreline Analysis System), see Moore (2000).

**Fig. 11.** Evidence of coastal current circulation oriented from east to west. (a) Wind rose established from data obtained by the Météo France record station at Brignogan over the period 1984–2007 (from Suanez et al., 2012). (b) Aerial photograph taken on 1rst February, 1975 by the IGN at mid-tide showing wave crests oriented to west (source: IGNF_PVA_1-0__1975-02__C0415-0082_1975_EDFGOUGSENY_5918). (c) Aerial photograph taken on 14 August 1978 by the IGN during high tide (source: IGNF_PVA_1-0_1978-08-14_C0714-0073_GSNY_FR3012IR_0416) showing nearshore wave refraction processes with the arrows labeled 1 to 5 (modified from Suanez et al., 2012). (d) Tide current modeling by the LOPS (IFREMER) for the large spring tide of the November 6, 2021, at 11ham (simulation extracted from the MARC (*Modélisation et Analyse pour la Recherche Côtière*) data base available at https://marc.ifremer.fr/).

**Fig. 12.** Elevation of the hard layer along the 4 profiles located along the eastern (profiles 1, 2, and 3) and central (profile 4) parts of Vougot beach (a), (b), (c), (d). The grey lines represent the envelope of the profiles between the first and the last surveys. Photos (e) and (f) show the outcrops of peat layer and Pleistocene silt and pebble accumulations along profiles 1, 2, and 3 (source: S. Suanez - December 2021).

**Fig. 13.** Number of dune toe exceedance events per year during the 17-year study period. The bars represent all ($\Delta z_{exceedance} > 0$) and significant ($\Delta z_{exceedance} > 0.8$m) dune toe exceedance events. The significant dune toe exceedance threshold is the mean plus 0.5 times the standard deviation ($\Delta z_{exceedance} > 0.8$m), as identified in shaded gray in figure 10.

**Fig. 14.** Estimated (a) extreme water level (*EWL*) and (b) dune toe exceedance ($\Delta z_{exceedance}$) with a return periods ($X_t$) of 2 to 50 years, showing the fitted Gumbel distributions (red curves), 95% confidence intervals (shaded blue), and observed maximum annual values (black points).

**Table 1.** Lower limits used for the calculation of the dune and the beach/dune system sediment budgets. The distance is measured from the head of the profile, which defines the origin of each profile.

**Table 2.** Significant erosion phases measured and quantified for each of the 6 profiles, showing the most significant erosion on February 4, 2014 (shaded gray). The values are expressed in cubic meters per linear meter ($m^3$ l.$m.^{-1}$). The asterisk indicates that the erosive phase is not significant because the calculated sediment budget is close to the measurement error, as estimated from the statistical analysis (see section 3.1.).

**Table 3.** Significant events that simultaneously exceeded the 97th quantile wave height ($H_{m0}$) and observed high tide water level (tide + surge = HTWL). For each event, the date(s), storm (if named), maximum $H_{m0}$, $T_{m-1,0}$, energy flux, HTWL, incident wave direction (mean ± standard deviation) and estimated *EWL* are shown. Events in shaded gray also exceeded the wave energy flux threshold (Fig. 7b), and those in bold occurred during the survey periods showing significant erosion (Table 2).

**Table 4.** Non-exhaustive summary of shoreline erosion dynamics and/or barrier retreat, related to five of the most significant combined storm wave and high spring tide level events. The shaded lines refer to the present study, showing the maximum shoreline retreat for each event.

Table 1

| | dune/upper beach limit (m) | lower beach limit (m) |
|---|---|---|
| Profile 1 | 18 | 175 |
| Profile 2 | 18 | 150 |
| Profile 3 | 22 | 176 |
| Profile 4 | 22 | 200 |
| Profile 5 | 15 | 200 |
| Profile 6 | 13 | 200 |

Table 2

| Date of surveys | Prof. 1 | Prof. 2 | Prof. 3 | Prof. 4 | Prof. 5 | Prof. 6 |
|---|---|---|---|---|---|---|
| 21/02/2008-12/03/2008 | –9.2 | –8.5 | –12.2 | * | * | * |
| 07/02/2013-14/02/2013 | –3.3 | –3.5 | * | * | * | * |
| 21/11/2013-09/01/2014 | –4 | –4.2 | –4.3 | –3.7 | * | * |
| 09/01/2014-04/02/2014 | –14.5 | –11.2 | –11.6 | –13.4 | –5 | –1.9 |
| 16/02/2014-06/03/2014 | * | * | –12.8 | –4.6 | –2.4 | * |
| 16/12/2015-15/02/2016 | –5.5 | –3.9 | * | –2 | * | * |
| 08/12/2017-08/01/2018 | –7.2 | –4.3 | –4.5 | * | * | * |
| 15/01/2020-12/02/2020 | –6.3 | –11.5 | –8.2 | –8.1 | * | * |
| 12/02/2020-13/03/2020 | –3 | –5.8 | –14.9 | –4.3 | * | * |
| 19/10/2020-20/11/2020 | –3.2 | * | –3.8 | –2.3 | * | * |

Table 3

| date | name | peak $H_{m0}$ (m) | max $T_{m-1,0}$ (s) | max energy flux (J/m.s) | max HTWL (m) | mean ± Std Dir (deg) | *EWL* (m) |
|---|---|---|---|---|---|---|---|
| **10/03/2008** | **Johanna** | **8.9** | **16.6** | **13.4 $10^5$** | **4.8** | **-46±4** | **8.6** |
| 31/03/2010 | | 5.0 | 10.4 | 2.7 $10^5$ | 4.7 | -61±13 | 6.9 |
| **01-02/02/2014** | **Anne** | **7.1** | **13.4** | **8.2 $10^5$** | **4.8** | **-49±7** | **9.6** |
| **28/02-03/03/2014** | **Christine** | **7.1** | **16.4** | **7.7 $10^5$** | **4.8** | **-48±7** | **8.7** |
| **08-10/02/2016** | **Imogen** | **8.3** | **16.8** | **10.2 $10^5$** | **4.5** | **-46±3** | **9.0** |
| **13/02/2016** | | 6.6 | 12.6 | 4.7 $10^5$ | 4.6 | -50±8 | 7.9 |
| 09/03/2016 | | 5.2 | 11.0 | 4.110$^5$ | 4.5 | -40 ± 10 | 6.8 |
| **03-04/01/2018** | **Eleanor** | **7.4** | **15.0** | **8.4 $10^5$** | **4.5** | **-50±6** | **9.1** |
| 23/01/2019 | | 4.4 | 13.3 | 2.7 $10^5$ | 4.4 | -43±5 | 7.8 |
| **13/02/2020** | Inès | 6.2 | 17.6 | 5.6 $10^5$ | 4.6 | -47±6 | 7.2 |
| **15/11/2020** | | 5.1 | 13.6 | 3.5 $10^5$ | 4.6 | -52±6 | 8.6 |

Table 4

| | | | |
|---|---|---|---|
| March 10, 2008 (Johanna storm) | Banneg island (Molène Archipelago, Finistère) (Fichaut and Suanez, 2010; 2011) | West Brittany | inland displacement of cliff top storm deposits up to 50 to 90 m from the edge of the cliff |
| | Gravel beaches of the islands of Molène Archipelago (Finistère) (Suanez et al., 2011; Stéphan et al., 2017) | West Brittany | maximum shoreline erosion up to –16 m to –26 m (Lez ar Chrizienn Island) and –2,5 m (Trielen Island) |
| | Vougot beach (Finistère) (Suanez and Cariolet, 2010a; Suanez et al., 2012, 2015) | North Brittany | maximum shoreline erosion up to –6 m |
| | Boutrouilles beach (Finistère) (Suanez and Cariolet, 2010a) | North Brittany | maximum shoreline erosion up to –3 m |
| | Sandy beach of the bay of Goulven (Finistère) (Stéphan et al., 2018a) | North Brittany | maximum shoreline erosion up to –8 m |

| | | | |
|---|---|---|---|
| | Sandy bay of Saint-Michel-en-Grève (Côtes d'Armor) (Suanez and Stéphan, 2011) | North Brittany | maximum shoreline erosion up to –17 m |
| | Gravel spit barrier of Sillon de Talbert (Côtes d'Armor) (Stéphan et al., 2010; 2012; 2018b; Suanez et al., 2018a) | North Brittany | maximum spit landward retreat up to –22 m |
| Winter 2013-2014 | Banneg island (Molène Archipelago, Finistère) (Autret et al., 2016) | West Brittany | inland displacement of cliff top storm deposits up to 50 to 90 m from the edge of the cliff |
| | Gravel beaches of the islands of Molène Archipelago (Finistère) (Blaise et al., 2015; Stéphan et al., 2017) | West Brittany | maximum shoreline erosion up to –4 m to –7 m (Trielen and Quéménez Islands respectively), and –13 m (Lez ar Chrizienn Island) |
| | Sandy beach of Vougot (Finistère) (Suanez et al., 2015; Blaise et al., 2015; Masselink et al., 2016) | North Brittany | maximum spit landward retreat up to –14 m |
| | Sandy beach of Tréompan (Ploudalmézeau, Finistère) (Stéphan et al., 2019a) | North Brittany | maximum spit landward retreat up to –14 m |
| | Boutrouilles beach (Finistère) (Blaise et al., 2015; Stéphan et al., 2019a) | North Brittany | maximum shoreline erosion up to –9 m |
| | Sillon de Talbert spit barrier (Côtes d'Armor) (Stéphan et al., 2018b; Suanez et al., 2018a, 2022) | North Brittany | maximum spit landward retreat up to –30 m |
| | Sandy beaches of Porsmilin and Blancs-Sablons (Finistère) – (Blaise et al., 2015; Stéphan et al., 2019a) | West Brittany | maximum shoreline erosion up to –19 m and –7 m respectively |
| | Sandy beaches of Penmarc'h and Treffiagat (Finistère) – (Blaise et al., 2015; Stéphan et al., 2019a) | South Brittany | maximum shoreline erosion up to –11 m to –14 m respectively |
| February 8, 2016 (Imogen) | Sillon de Talbert spit barrier (Côtes d'Armor) (Fichaut et al., 2017; Stéphan et al., 2018b; Suanez et al., 2018a, 2022) | North Brittany | maximum spit landward retreat up to –18 m |
| | Sandy beach of Vougot (Finistère) (Suanez et al., 2017) | North Brittany | maximum shoreline erosion up to –6 m |
| | Sandy beach of the bay of Goulven (Finistère) (Stéphan et al., 2018a) | North Brittany | maximum shoreline erosion up to –8 m (east) to –13 m (west) |
| January 3-4, 2018 (Eleanor) | Sillon de Talbert spit barrier (Côtes d'Armor) (Stéphan et al., 2019b; Suanez et al., 2022) | North Brittany | maximum spit landward retreat up to –12 m |
| | Sandy beach of Vougot (Finistère) (Suanez, 2019) | North Brittany | maximum shoreline erosion up to –2,5 m |
| February 10, 2020 (Ciara) | Sillon de Talbert spit barrier (Côtes d'Armor) (Stéphan et al., 2020; Suanez et al., 2022) | North Brittany | maximum spit landward retreat up to –16 m |
| | Sandy beach of Vougot (Finistère) (Suanez, 2021) | North Brittany | maximum shoreline erosion up to –6 m |

**Declaration of interests**

☐The authors declare that they have no known competing financial interests or personal relationships that could have appeared to influence the work reported in this paper.

☒The authors declare the following financial interests/personal relationships which may be considered as potential competing interests:

Serge Suanez reports financial support was provided by Université de Bretagne Occidentale.

.

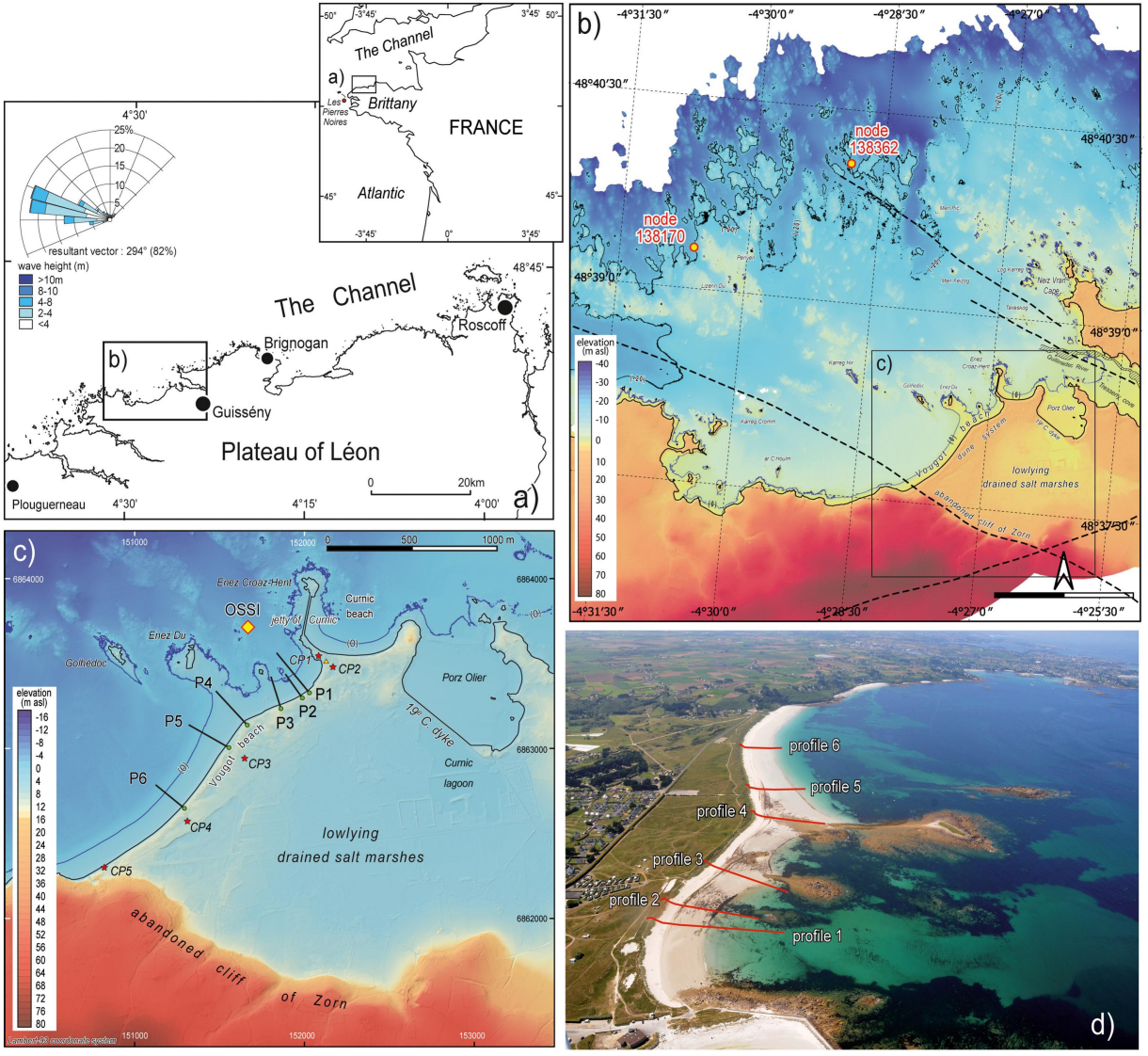
a)
The Channel
Brittany
FRANCE
Les Pierres Noires
Atlantic
50°
45°
3°45'
0°
4°30'
25%
20
15
10
5
resultant vector : 294° (82%)
wave height (m)
>10m
8-10
4-8
2-4
<4
The Channel
48°45'
Roscoff
Brignogan
b)
Guissény
Plateau of Léon
Plouguerneau
4°30'
4°15'
4°00'
0
20km
a)
b)
-4°31'30"
-4°30'0"
-4°28'30"
-4°27'0"
48°40'30"
node 138362
node 138170
48°39'0"
elevation (m asl)
-40
-30
-20
-10
0
10
20
30
40
50
60
70
80
c)
Vougot beach dune system
lowlying drained salt marshes
abandoned cliff of Zorn
48°37'30"
-4°25'30"
c)
151000
152000
153000
0
500
1000 m
6864000
6863000
6862000
Enez Croaz-Hent
OSSI
jetty tip Cumic
Cumic beach
Enez Du
Golhédoc
CP1
CP2
P1
P2
P3
P4
P5
P6
Porz Olier
19th C dyke
Cumic lagoon
Vougot beach
CP3
CP4
CP5
lowlying drained salt marshes
abandoned cliff of Zorn
elevation (m asl)
-16
-12
-8
-4
0
4
8
12
16
20
24
28
32
36
40
44
48
52
56
60
64
68
72
76
80
Lambert-93 coordinate system
profile 6
profile 5
profile 4
profile 3
profile 2
profile 1
d)

Figure 1

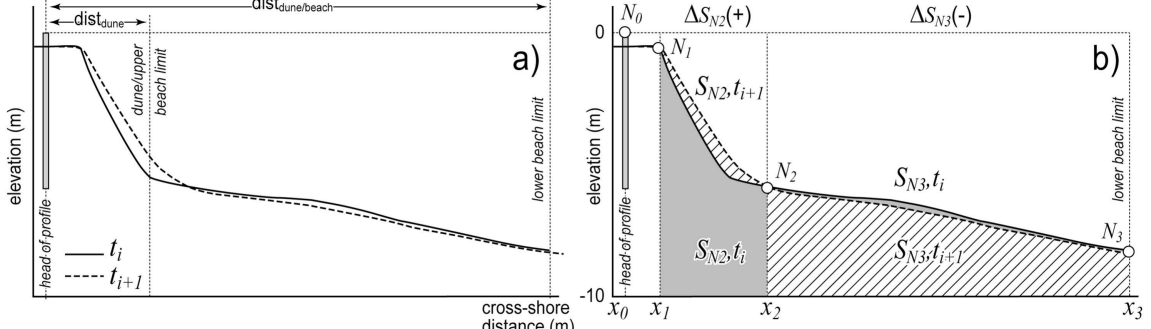
dist_dune/beach
dist_dune
a)
dune/upper beach limit
lower beach limit
elevation (m)
head of profile
t_i
t_i+1
cross-shore distance (m)
N_0
ΔS_N2(+)
ΔS_N3(-)
b)
0
-10
N_1
S_N2,t_i+1
N_2
S_N3,t_i
N_3
S_N2,t_i
S_N3,t_i+1
x_0
x_1
x_2
x_3

Figure 2

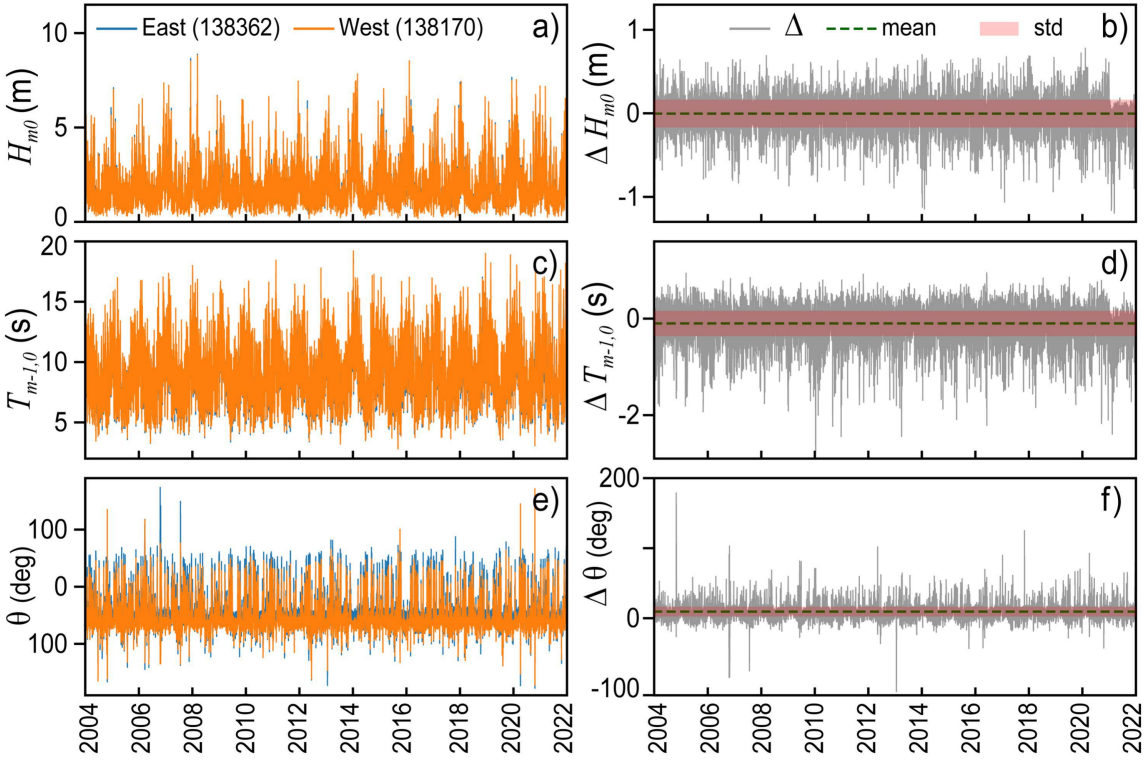
East (138362)
West (138170)
a)
$H_{m0}$ (m)
b)
Δ
mean
std
Δ $H_{m0}$ (m)
c)
$T_{m-1,0}$ (s)
d)
Δ $T_{m-1,0}$ (s)
e)
θ (deg)
f)
Δ θ (deg)
2004
2006
2008
2010
2012
2014
2016
2018
2020
2022

Figure 3

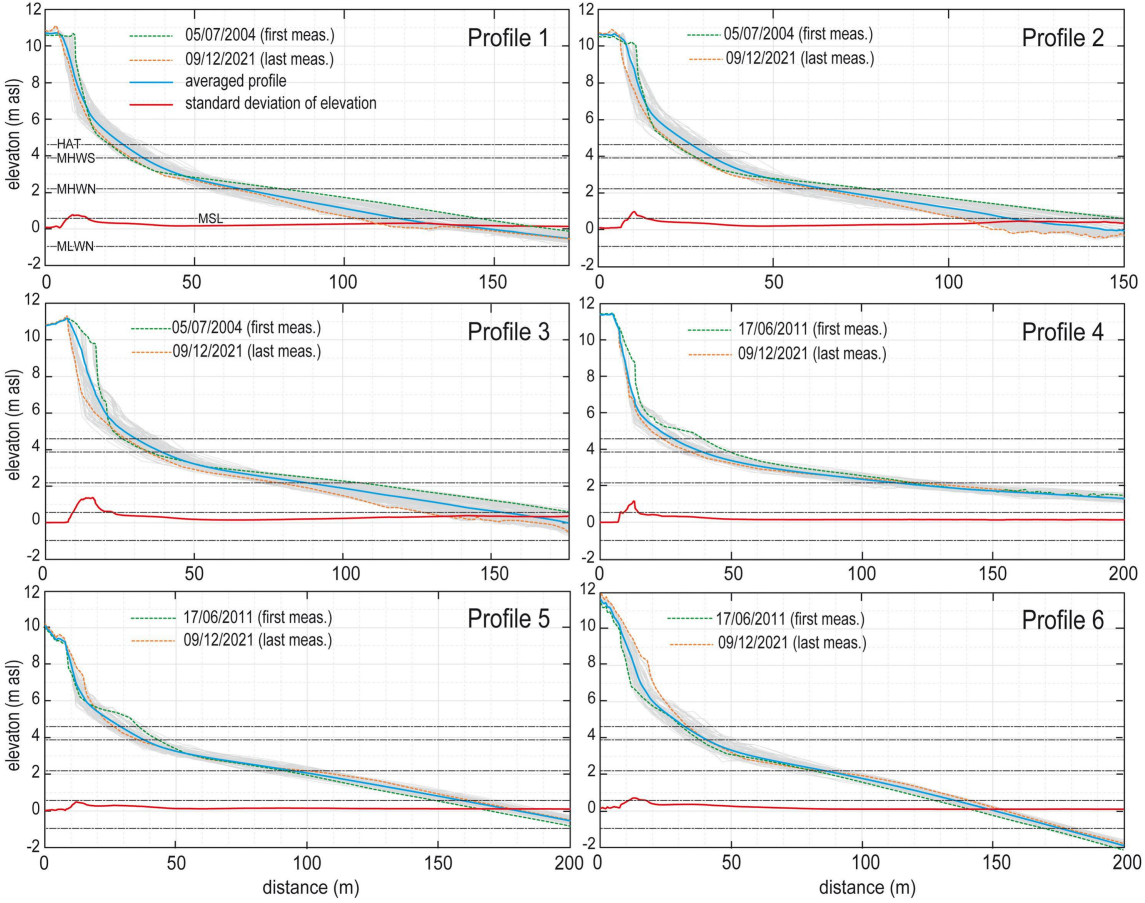
Profile 1
05/07/2004 (first meas.)
09/12/2021 (last meas.)
averaged profile
standard deviation of elevation
HAT
MHWS
MHWN
MSL
MLWN
elevaton (m asl)
Profile 2
05/07/2004 (first meas.)
09/12/2021 (last meas.)
Profile 3
05/07/2004 (first meas.)
09/12/2021 (last meas.)
Profile 4
17/06/2011 (first meas.)
09/12/2021 (last meas.)
Profile 5
17/06/2011 (first meas.)
09/12/2021 (last meas.)
Profile 6
17/06/2011 (first meas.)
09/12/2021 (last meas.)
distance (m)

Figure 4

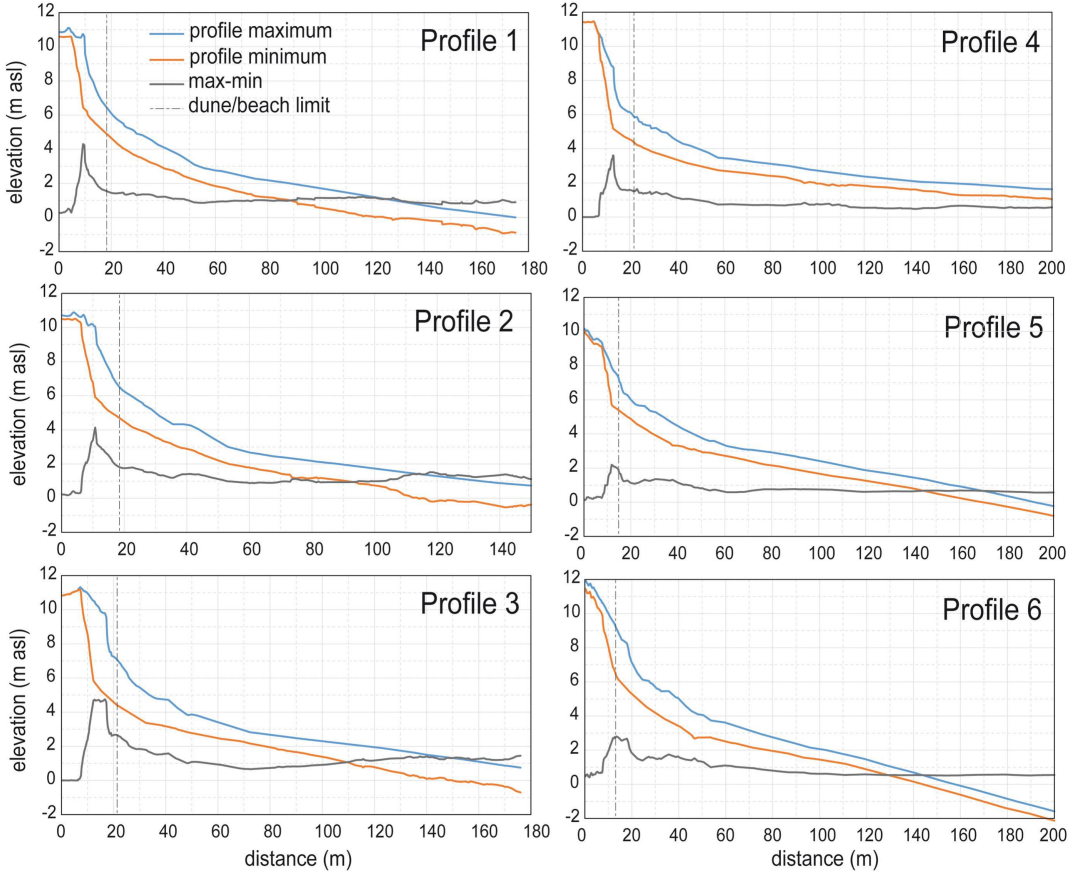
profile maximum
profile minimum
max-min
dune/beach limit
Profile 1
Profile 2
Profile 3
Profile 4
Profile 5
Profile 6
elevation (m asl)
distance (m)

Figure 5

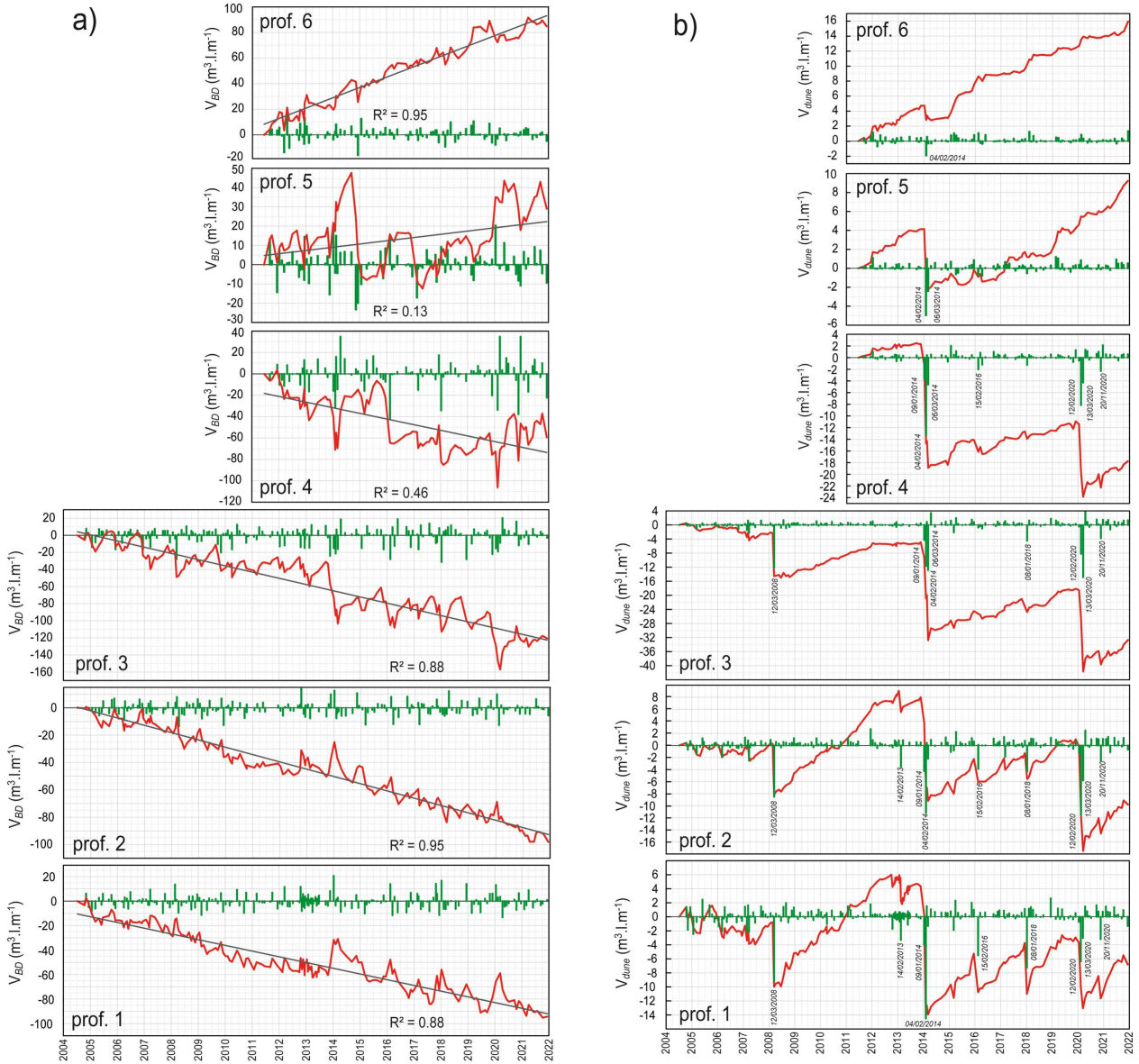
a)
b)
prof. 6
prof. 5
prof. 4
prof. 3
prof. 2
prof. 1
$V_{BD}$ (m³.l.m⁻¹)
$V_{dune}$ (m³.l.m⁻¹)
R² = 0.95
R² = 0.13
R² = 0.46
R² = 0.88
R² = 0.95
R² = 0.88
04/02/2014
06/03/2014
08/01/2014
15/02/2016
12/02/2020
13/3/2020
20/11/2020
12/03/2008
14/02/2013
08/01/2018
2004
2005
2006
2007
2008
2009
2010
2011
2012
2013
2014
2015
2016
2017
2018
2019
2020
2021
2022

Figure 6

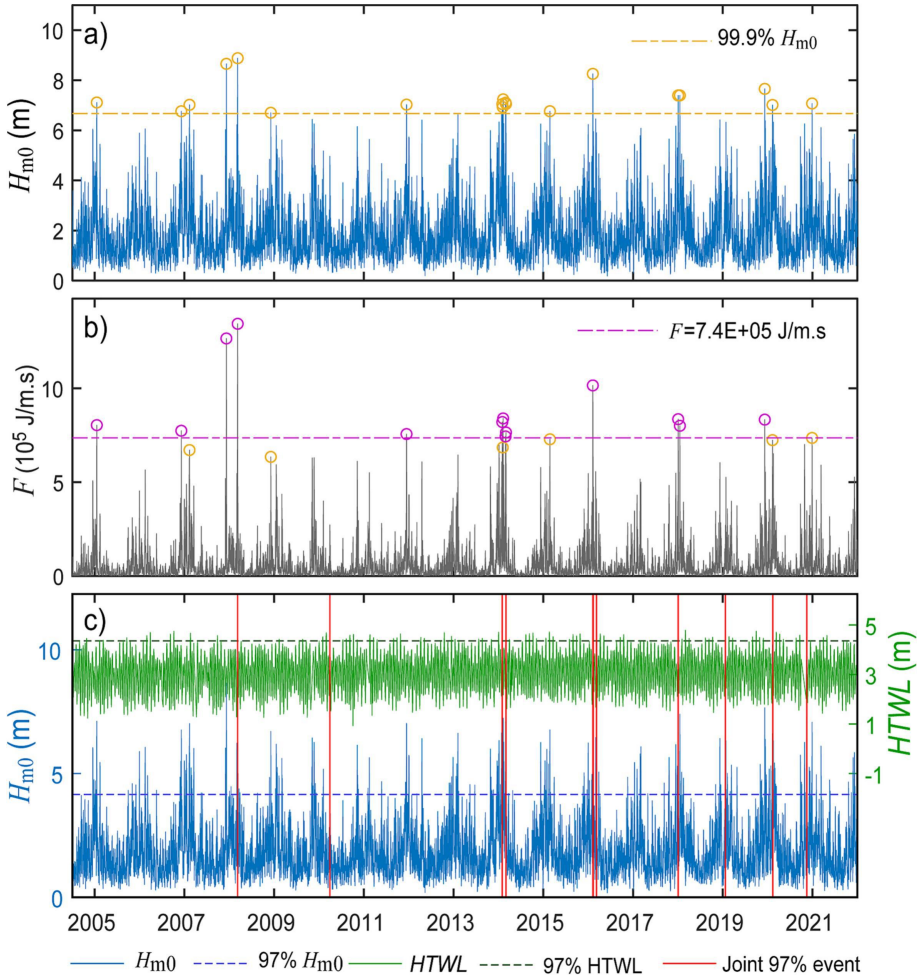
a)
99.9% $H_{m0}$
$H_{m0}$ (m)
b)
$F$=7.4E+05 J/m.s
$F$ ($10^5$ J/m.s)
c)
$H_{m0}$ (m)
*HTWL* (m)
2005
2007
2009
2011
2013
2015
2017
2019
2021
$H_{m0}$
97% $H_{m0}$
*HTWL*
97% HTWL
Joint 97% event

Figure 7

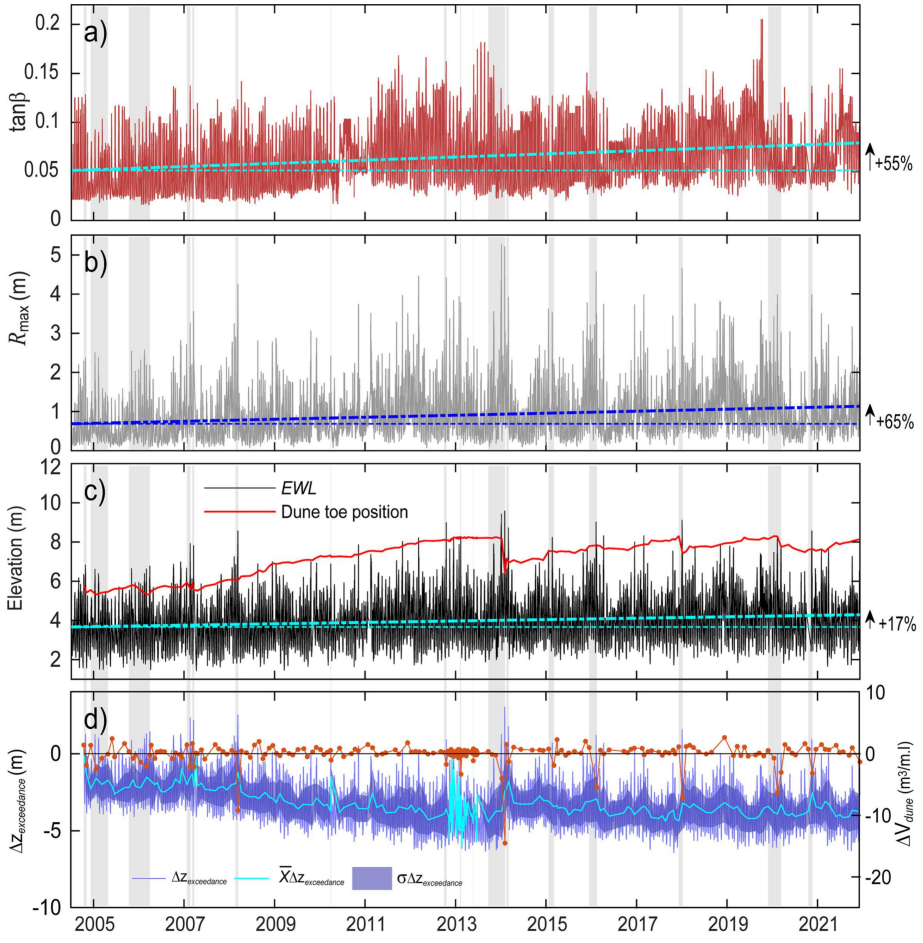
a)
tanβ
+55%
b)
$R_{max}$ (m)
+65%
c)
EWL
Dune toe position
Elevation (m)
+17%
d)
$\Delta z_{exceedance}$ (m)
$\Delta V_{dune}$ (m³/m.l)
$\Delta z_{exceedance}$
$\overline{X}\Delta z_{exceedance}$
$\sigma\Delta z_{exceedance}$
2005
2007
2009
2011
2013
2015
2017
2019
2021

Figure 8

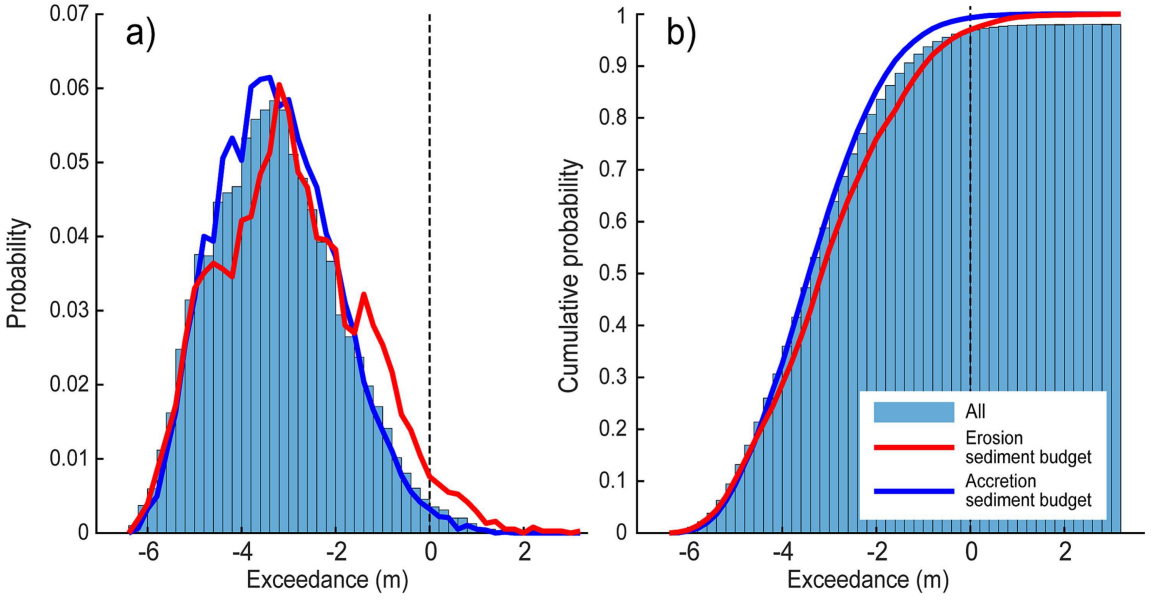
a)
b)
Probability
Cumulative probability
Exceedance (m)
Exceedance (m)
All
Erosion
sediment budget
Accretion
sediment budget

Figure 9

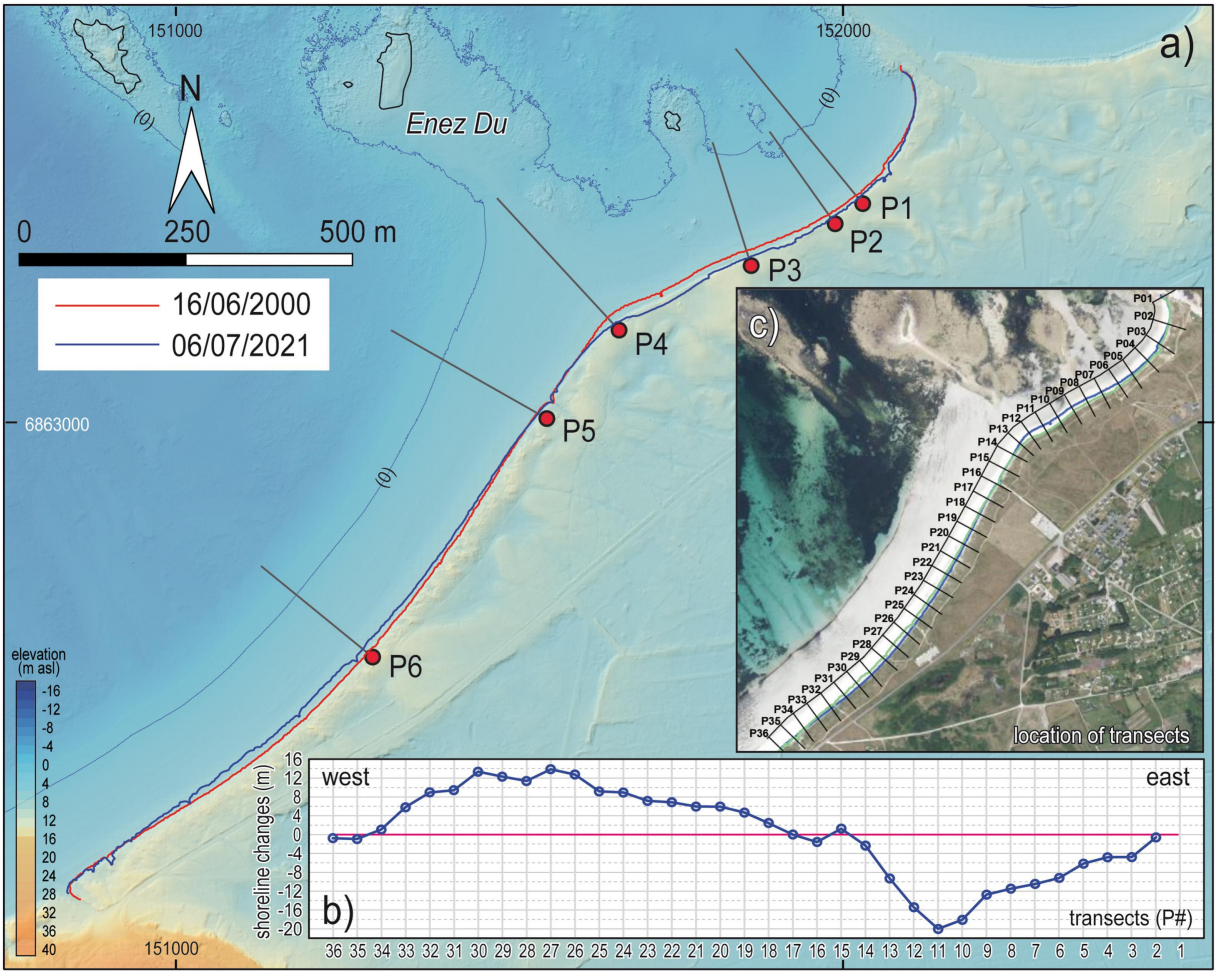
a)
151000
152000
N
Enez Du
0
250
500 m
16/06/2000
06/07/2021
6863000
P1
P2
P3
P4
P5
P6
elevation (m asl)
-16
-12
-8
-4
0
4
8
12
16
20
24
28
32
36
40
c)
location of transects
shoreline changes (m)
west
east
b)
transects (P#)

Figure 10

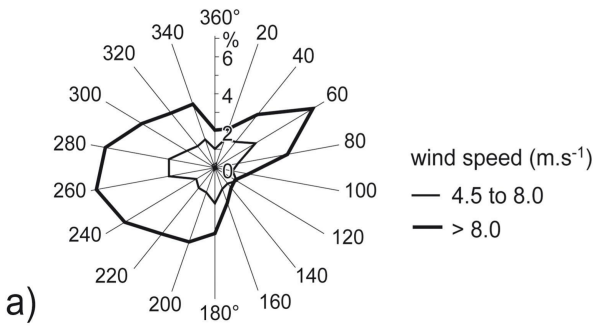
a)
360°
%
6
4
2
0
20
40
60
80
100
120
140
160
180°
200
220
240
260
280
300
320
340
wind speed (m.s-1)
4.5 to 8.0
> 8.0

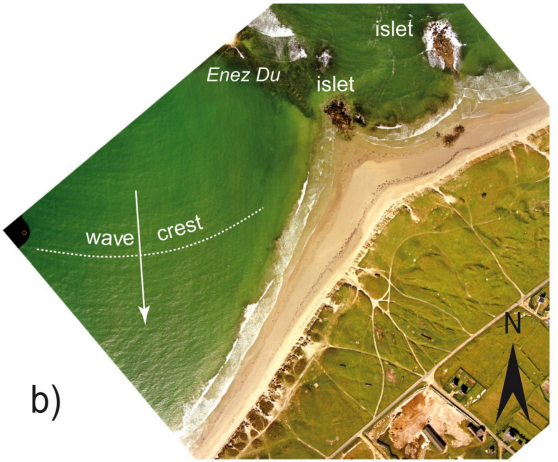
b)
islet
Enez Du
islet
wave
crest
N

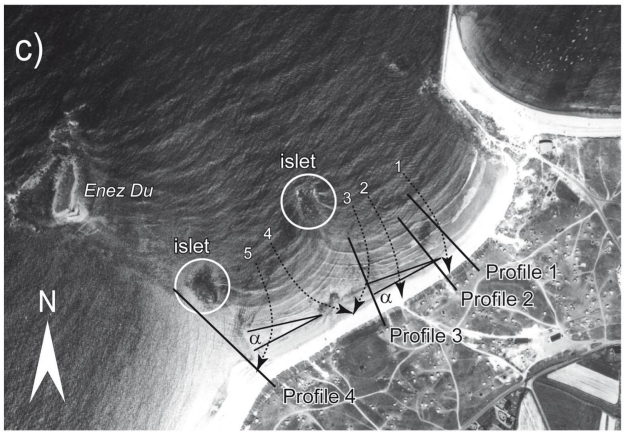
c)
Enez Du
islet
islet
1
2
3
4
5
Profile 1
Profile 2
Profile 3
Profile 4
α
α
N

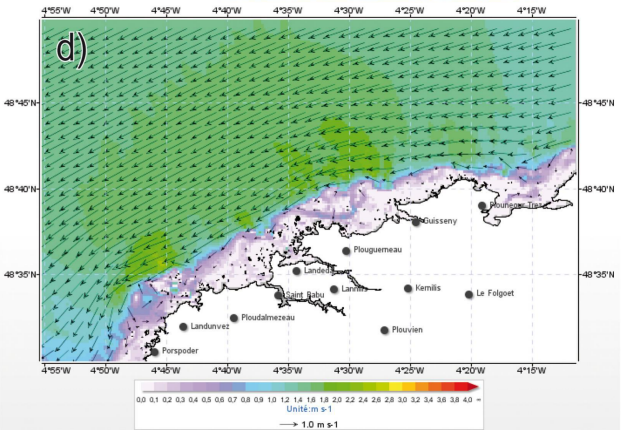
d)
4°55'W
4°50'W
4°45'W
4°40'W
4°35'W
4°30'W
4°25'W
4°20'W
4°15'W
48°45'N
48°40'N
48°35'N
Guisseny
Plouguerneau
Landeda
Saint Pabu
Lanrivoaré
Kernilis
Le Folgoet
Ploudalmezeau
Landunvez
Plouvien
Porspoder
Unité m s-1
1.0 m s-1

Figure 11

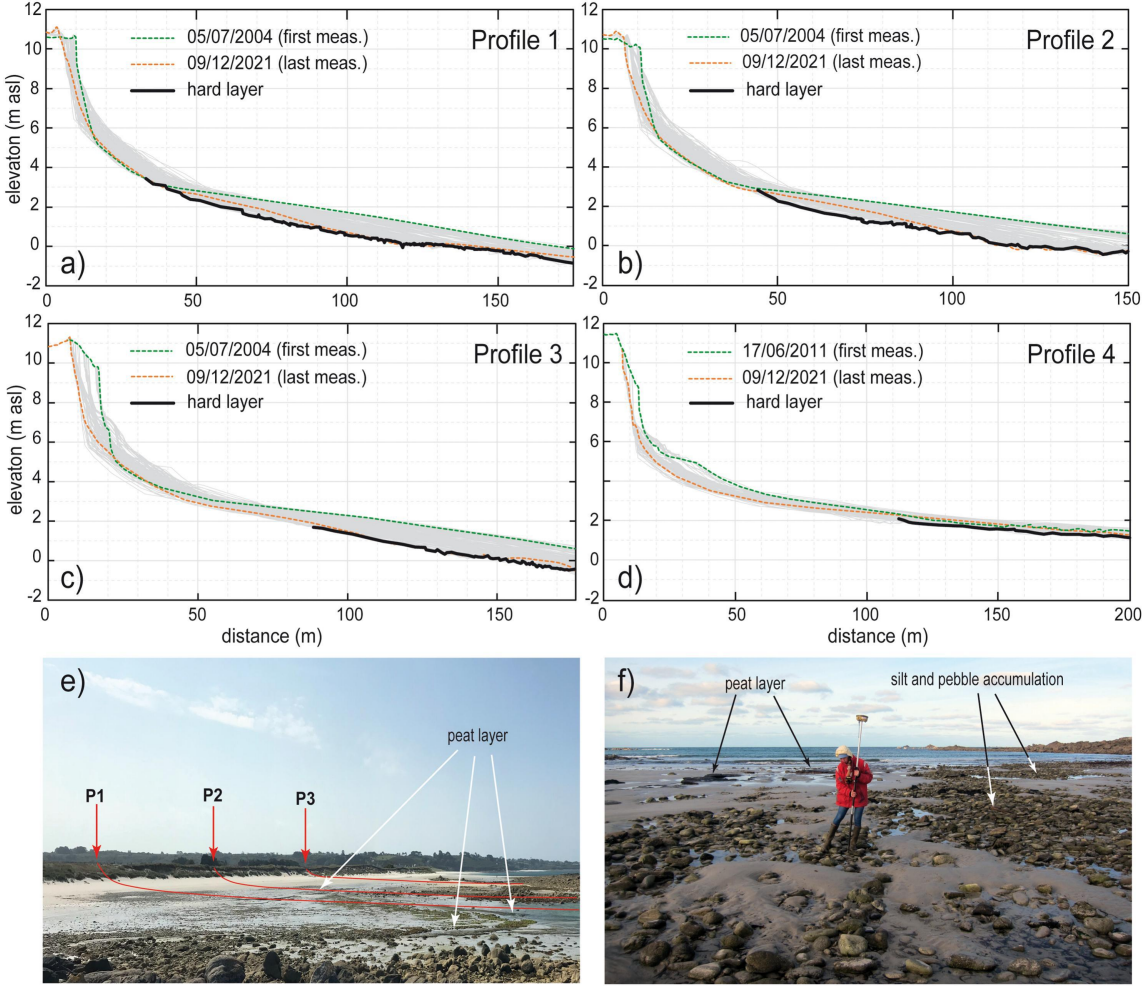
Profile 1
05/07/2004 (first meas.)
09/12/2021 (last meas.)
hard layer
elevaton (m asl)
a)
Profile 2
05/07/2004 (first meas.)
09/12/2021 (last meas.)
hard layer
b)
Profile 3
05/07/2004 (first meas.)
09/12/2021 (last meas.)
hard layer
elevaton (m asl)
c)
distance (m)
Profile 4
17/06/2011 (first meas.)
09/12/2021 (last meas.)
hard layer
d)
distance (m)
e)
peat layer
P1
P2
P3
f)
peat layer
silt and pebble accumulation

Figure 12

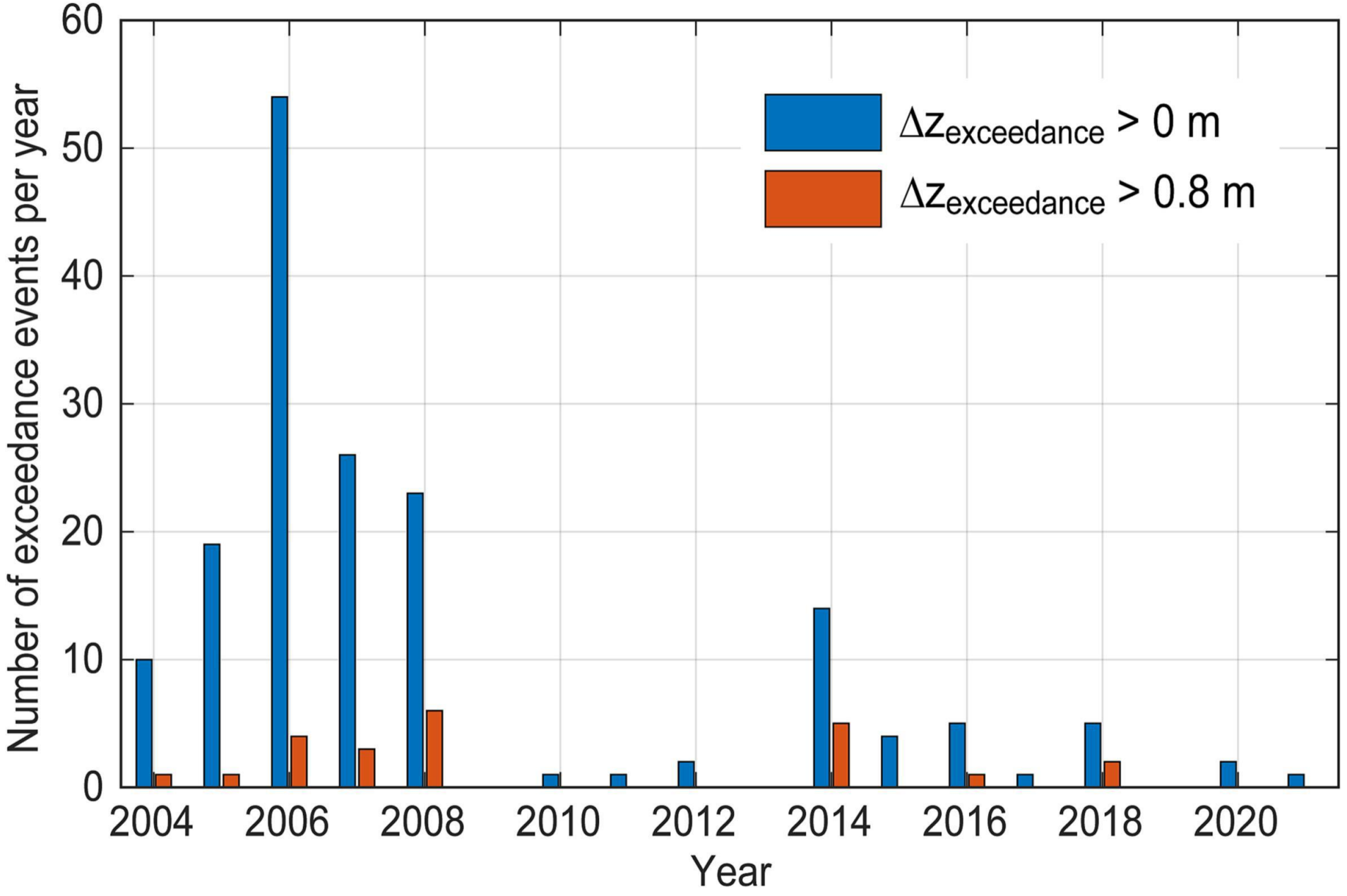
Number of exceedance events per year
Year
$\Delta z_{exceedance}$ > 0 m
$\Delta z_{exceedance}$ > 0.8 m
0
10
20
30
40
50
60
2004
2006
2008
2010
2012
2014
2016
2018
2020

Figure 13

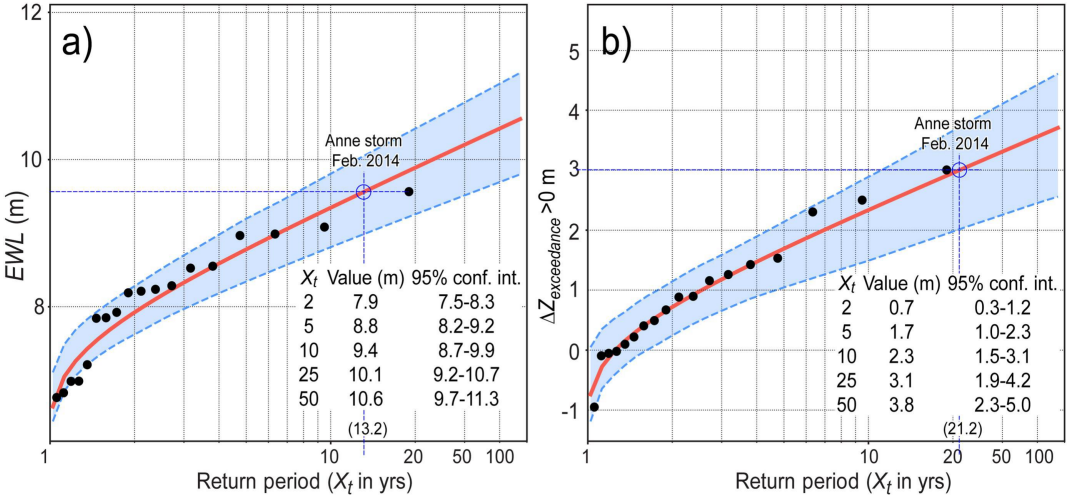
a)
Anne storm
Feb. 2014
$X_t$ Value (m) 95% conf. int.
2 7.9 7.5-8.3
5 8.8 8.2-9.2
10 9.4 8.7-9.9
25 10.1 9.2-10.7
50 10.6 9.7-11.3
(13.2)
EWL (m)
Return period ($X_t$ in yrs)
b)
Anne storm
Feb. 2014
$X_t$ Value (m) 95% conf. int.
2 0.7 0.3-1.2
5 1.7 1.0-2.3
10 2.3 1.5-3.1
25 3.1 1.9-4.2
50 3.8 2.3-5.0
(21.2)
$\Delta Z_{exceedance}$ >0 m
Return period ($X_t$ in yrs)

Figure 14